Available online at www.sciencedirect.com
SCIENCE DIRECT®
Physics of the Earth and Planetary Interiors 138 (2003) 197–222
PHYSICS OF THE EARTH AND PLANETARY INTERIORS
www.elsevier.com/locate/pepi

# Inferring upper-mantle temperatures from seismic velocities

Fabio Cammarano [a,*], Saskia Goes [a], Pierre Vacher [b], Domenico Giardini [a]

[a] *Institute of Geophysics, ETH Hoenggerberg (HPP), Zurich, Switzerland*
[b] *Laboratoire de Geophysique et Planétologie, Université de Nantes, Nantes, France*

Received 7 October 2002; received in revised form 4 June 2003; accepted 2 July 2003

**Abstract**

Constraints on mantle temperatures are fundamental for a better understanding of the dynamics of the Earth. We evaluate how well upper-mantle thermal structure can be inferred from seismic velocities. Our forward calculation of seismic velocities and density includes uncertainties in anharmonic and anelastic parameters for various compositional models. The sensitivity of $V_P$ ($V_S$) to temperature along a 1300 °C adiabat decreases with depth from $-0.75\pm0.15\%$ ($1.3\pm0.30\%$) per 100 °C at 200 km, to $-0.23\pm0.05\%$ ($-0.45\pm0.10\%$) per 100 °C at 800 km, with an additional reduction in the wadsleyite stability zone. Shear anelasticity introduces a significant non-linear dependence of seismic velocities on temperature in the upper-mantle. This means that seismic anomalies with similar amplitudes but different signs correspond to temperature anomalies of a different magnitude, and absolute seismic velocities are required for making a thermal interpretation. With depth, the importance of anelasticity decreases. Temperature derivatives of bulk sound velocity ($V_\phi$) and density ($\rho$) are a factor two to five lower than those of $V_{P,S}$ and do not depend strongly on temperature. Common mantle compositions cause velocity anomalies of about 1% throughout the upper-mantle. Above 400 km depth, the effect of composition on $V_P$ and $V_S$ is secondary to the effect of temperature, but it gains importance with increasing depth. For most upper-mantle compositions and depths, the relative sensitivity of $V_P$, $V_S$ and $V_\phi$ to temperature and composition is not different enough to distinguish the two factors from combined velocity models. But $\partial\ln\rho/\partial\ln V_S$ allows a separation of thermal anomalies from compositional anomalies for iron-depleted and subducted material. Spherically symmetric reference profiles underlie most seismic velocity models. However, small differences between common one-dimensional velocity models translate into disparate thermal interpretations. A better understanding of seismic uncertainties and the physical interpretation of reference models is necessary to interpret absolute velocities. Assuming seismic structure is well resolved and composition known, uncertainties in inferred thermal structure are ±100 °C above 400 km depth and ±250 °C in the shallow lower-mantle. This makes an inversion of seismic velocity models for temperature feasible, above 400 km depth. At larger depths, testing seismic velocities calculated for a proposed thermal and compositional structure against observations is a more promising interpretation approach.


*Keywords:* Upper-mantle; Elasticity and anelasticity; Thermal structure; Seismic velocities

## 1. Introduction

Dynamics and rheology of the Earth's mantle are governed by pressure–temperature conditions and

* Corresponding author. Tel.: +41-1-633-4075; fax: +41-1-633-1065.
*E-mail address:* fabio@tomo.ig.erdw.ethz.ch (F. Cammarano).

0031-9201/$ – see front matter © 2003 Elsevier B.V. All rights reserved.
doi:10.1016/S0031-9201(03)00156-0

composition. Up to now, our knowledge of mantle thermal and compositional structure is limited. The best constraints come from combining seismic models with mineral physics data. There is a long history of interpreting one-dimensional seismic models in terms of the Earth's physical state (e.g. Birch, 1952; Davies and Dziewonski, 1975; Duffy and Anderson, 1989; Ita and Stixrude, 1992; Jackson and Ridgen, 1998; Vacher et al., 1998; Weidner, 1985). To a first-order, adiabacity and olivine phase-transitions can explain spherically-symmetric seismic models of the mantle. But deviations from this average structure reflect the mantle's dynamics. As techniques to reconstruct three-dimensional seismic structure at a global, regional and local scale improve, the thermal interpretation of such models is becoming pertinent (Deal et al., 1999; Forte et al., 1995; Forte and Mitrovica, 2001; Humphreys and Dueker, 1994; Lithgow-Bertelloni, 2001; Murakami and Yoshioka, 2001; Nolet and Zielhuis, 1994; Sobolev et al., 1996, 1997; Tralli and Ita, 1995). For interpretation efforts, a systematic assessment of uncertainties in converting seismic velocities to thermal structure is important.

An evaluation of uncertainties in elastic and anelastic parameters in the uppermost mantle has shown that the inversion of seismic velocities can provide temperature estimates within $\pm 100\,^{\circ}\mathrm{C}$ down to about 200 km depth (Goes et al., 2000; Sobolev et al., 1996). The effect of composition on seismic velocities can, to a first-order, be neglected in the shallow mantle below the crust. In this depth range, consistent temperature estimates can be obtained from $V_P$ and $V_S$ where the resolution of the seismic images is good (Goes et al., 2000; Goes and van der Lee, 2002). Density does have a significant sensitivity to composition. Combined interpretations of gravity and seismic data recover compositional structure, for example, below cratons (Deschamps et al., 2001, 2002; Forte et al., 1995; Forte and Perry, 2000).

When parameters are extrapolated to lower-mantle conditions uncertainties increase and the sensitivity to composition becomes of the same order of the sensitivity to thermal structure (Jackson, 1998; Karato and Karki, 2001; Trampert et al., 2001). Heterogeneity ratios ($\partial \ln V_S/\partial \ln V_P$, $\partial \ln V_\phi/\partial \ln V_S$ and $\partial \ln \rho/\partial \ln V_S$, which describe the relative sensitivity of S- versus P-velocity, bulk sound versus S-velocity and density versus S-velocity, respectively) can be used for discriminating thermal and compositional effects in the lower-mantle (Karato and Karki, 2001; Trampert et al., 2001). No such sensitivity analysis has been done in the upper-mantle below about 200 km depth.

Here we evaluate the potential of using upper-mantle seismic velocities to infer the mantle's physical state, with emphasis on its temperature structure. The large experimental data base and ab initio calculations of the elastic properties of upper-mantle minerals allow for the forward calculation of elastic velocities and density for various compositions and pressure–temperature ($P$–$T$) conditions with reasonable confidence (Duffy and Anderson, 1989; Jackson and Ridgen, 1998; Karato and Karki, 2001; Vacher et al., 1998). The effect of anelasticity is often neglected in such calculations. However, anelasticity is important at seismic frequencies and can be included using a formulation based on the few laboratory data available and constrained by spherically-symmetric seismic attenuation models (Karato, 1993; Karato and Karki, 2001). As a result of anelasticity, seismic velocities depend non-linearly on temperature. Therefore, velocity anomalies cannot be interpreted directly, but need to be converted to absolute velocities. Uncertainties in the synthetic absolute velocities and density for a depth range of 200–800 km are determined, using published mineral physics data and third-order finite-strain and Grüneisen theory for the extrapolation to high pressure and temperature. Temperature and composition are the main parameters controlling lateral variations in isotropic seismic velocities. The sensitivity of seismic velocities and density to both parameters is discussed. Subsequently, the feasibility of interpreting upper-mantle seismic structure is assessed. Specifically, we discuss: (1) how uncertainties in forward calculated seismic parameters translate into temperature uncertainties; (2) the effect that reference models may have on thermal interpretation of absolute seismic structure; (3) the potential for separating thermal and compositional effects. We focus our analysis on uncertainties associated with mineral physics data. Limited resolution of the seismic models due to data coverage and sensitivity, model parameterization, and errors in the data add to the uncertainty of any interpretation, but have to be evaluated for each model individually.

## 2. Method

The forward calculation of seismic velocities and density as a function of pressure and temperature is a two-step procedure that requires the following data:

- Anharmonic (elastic) data for each mineral phase, i.e. density at ambient condition ($\rho_0$), thermal expansivity ($\alpha$), the elastic adiabatic bulk modulus ($K_S$) and shear modulus ($G$) and their pressure and temperature derivatives, and heat capacity ($C_P$)
- Anelastic parameters consisting of the frequency dependence of the attenuation ($a$), solidus temperature ($T_m(P)$) or activation volume ($V$), activation enthalpy ($H$) and a factor ($B$) that sets the amplitude of the anelastic model.
- Starting compositional models and summary phase diagrams to determine the evolution of composition with increasing pressure and temperature.

Parameter uncertainties have been estimated and are summarised in Table A.1 for the elastic parameters and in the Section 2.2 for anelasticity. To determine uncertainties in seismic velocities and density, we perform a large number (2200) of calculations with anharmonic and anelastic parameters randomly chosen within their range. This procedure does not evaluate uncertainties that the chosen equation of state (EOS) introduces. The choice can become important at lower-mantle pressures and temperatures (e.g. Jackson, 1998; Poirier and Tarantola, 1998; Stacey and Isaak, 2001), where few data are available to test extrapolation results. However, at upper-mantle conditions, the equation of state has a relatively small effect as long as the extrapolation is consistent with available data at higher pressure and temperature conditions (e.g. Jackson and Ridgen, 1998).

### 2.1. Anharmonicity

The first step of the calculation determines density and anharmonic (i.e. elastic) moduli $K_S$ and $G$ for each single mineral, using Grüneisen's theory for the extrapolation to high temperature, and third-order finite-strain theory for the extrapolation in pressure along adiabats. The equations used are reported in Appendix A. Hashin–Strikman averaging gives parameters for a composite mineralogy. This procedure is the same as used by Vacher et al. (1996, 1998) with a few modifications. First, pressure extrapolation is done more appropriately along individual mineral adiabats rather than along one composite adiabat (Trampert et al., 2001). Second, we use a linear extrapolation for the high temperature corrections of the elastic moduli. This provides a better fit to available experimental data (Jackson et al., 2000; Katsura et al., 2001; Li et al., 2001) than a non-linear extrapolation based on the assumption that the Anderson–Grüneisen parameter does not vary with temperature (Duffy and Anderson, 1989). Third, and most important, we updated the mineral elasticity data set ($\rho_0$, $K_S$, $G$ and their $P$ and $T$ derivatives) using the results from recent high $P$–$T$ measurements and ab initio theoretical calculations (Appendix B, Table A.1).

Details about the compilation of the data are given in Appendix B. Here we just make a few remarks. To be consistent with our third-order finite-strain pressure extrapolation, only parameters that were derived from a third-order finite-strain EOS were included. This EOS works well for most minerals under upper and shallow lower-mantle conditions (the few exceptions are marked in Table A.1). The uncertainty range of the anharmonic parameters has been estimated by comparing different experiments. Where no experimental data are available (as, for instance, for many temperature derivatives) we adopt large uncertainties. Thermal expansion ($\alpha$) and heat capacity ($C_P$) of the mantle minerals are from the compilation of Saxena and Shen (1992), except the $\alpha$ value for Ca-perovskite (Wang et al., 1996) and $\alpha$ and $C_P$ for perovskite (model 2 in Saxena et al., 1999). $\alpha$ and $C_P$ are given in terms of polynomials of temperature and were assessed by a consistent thermodynamic procedure (Saxena and Shen, 1992). Errors of 20% are assumed for $\alpha$ for all minerals. $C_P$ is much better constrained and only used in the calculation of adiabats. Uncertainties in $C_P$ (about 1%) and in the adiabats (about 15 °C) were neglected in further analyses.

### 2.2. Anelasticity

The second step is to include anelastic effects (see also Appendix A). Viscoelastic relaxation at high temperature leads to dispersion (frequency dependence of seismic wave speeds) and dissipation (attenuation). Anelasticity is strongly temperature dependent and its

effect cannot be neglected in the interpretation of seismic velocities (Karato, 1993).

Shear anelasticity due to viscoelastic relaxation can be expressed as

$$Q_S = B\omega^a \exp\left(\frac{aH(P)}{RT}\right) \quad \text{with} \quad H(P) = E + PV$$

where $B$ is a normalization factor, $\omega$ the seismic frequency, $a$ the exponent describing the frequency dependence of the attenuation, $T$ the temperature, $R$ the gas constant, $E$ the activation energy, $V$ the activation volume and $H$ the activation enthalpy. A useful homologous temperature scaling is (Karato, 1993)

$$g = \frac{H(P)}{RT_m(P)}$$

where the dimensionless factor $g$ is a function of the activation enthalpy $H$, the melting temperature $T_m$ and the gas constant $R$. Although it does not have a substantial basis in seismic-frequency experimental data (Jackson, 2000), the extrapolation of $Q_S$ to high pressure using the melting temperature has been favoured, because it overcomes the lack of reliable data for the pressure dependence of the activation enthalpy. We assume bulk attenuation to be large and constant ($Q_K = 1000$ in the upper and 10,000 in the lower-mantle), consistent with seismic observations (Durek and Ekstrom, 1996).

To define a model of the seismic anelasticity and its uncertainties, we use constraints on attenuation coming from seismological observations (Romanowicz and Durek, 2000) as well as data available from laboratory measurements (Jackson, 2000; Tan et al., 2001). We choose a two-pronged approach. The first strategy uses the homologous temperature scaling for high-pressure extrapolation and seismic attenuation constraints to assess the pre-exponential factor. An alternative strategy, based almost completely on mineral physics data, expresses the pressure dependence of $Q_S$ in terms of activation volume. We define eight models of $Q_S$ in the upper-mantle and shallow lower-mantle (Fig. 1, parameters in Table 1): six models with the first approach (Q1–Q6) and two models with the second approach (Q7, Q8). These models are meant to be representative for an average mantle composition. The frequency is fixed at 1 Hz, consistent with the seismic frequency of PREM and AK135.

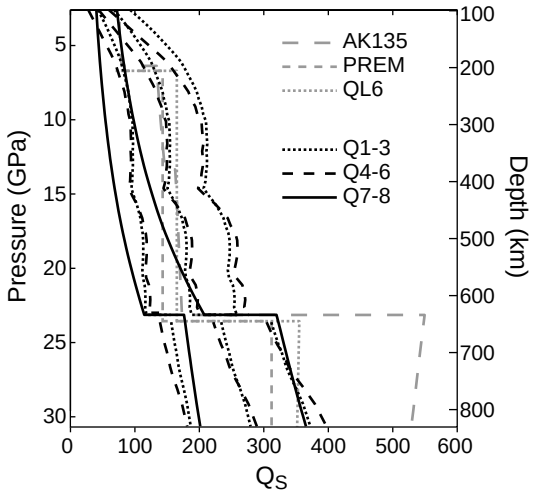


Fig. 1. Set of anelasticity models used for assessing uncertainties due to anelasticity. The models are constrained by laboratory and seismological data for the upper- and shallow lower-mantle and compared with the seismological one-dimensional attenuation models AK135 (Montagner and Kennett, 1996), PREM (Dziewonski and Anderson, 1981) and QL6 (Durek and Ekstrom, 1996). Parameters for the models are given in Table 1.

In the case of weak attenuation and its power law dependence on frequency, the anelastic correction of seismic velocity is proportional to the inverse quality factor, seismologically measured (Minster, 1980). In general, seismic attenuation is determined from free oscillation and surface wave data. Part of the seismically estimated $Q_S$ is probably due to scattering effects instead of intrinsic attenuation. The two effects are difficult to separate (Romanowicz and Durek, 2000) and for the purpose of this study we assume that the seismic $Q_S$ estimates reflect anelastical effects. Features that have been consistently found since the earliest models are the predominance of shear over bulk attenuation in most depth ranges and a weak frequency-dependence ($a$ between 0.1 and 0.4). Furthermore, there is a reasonable agreement between radial $Q_S$ models of the upper-mantle (Romanowicz and Durek, 2000).

The development of experimental techniques to measure the viscoelastic behaviour at high temperature and seismic frequencies is starting to provide direct constraints on shear attenuation phenomena in the Earth (Jackson, 1993, 2000). Experiments to date have been performed for only a few minerals,

Table 1
Anelasticity parameters

| Homologous temperature | $B^{a,b}$ ($s^a$) | | $g^a$ | | $a$ |
|---|---|---|---|---|---|
| Q1 | 0.5, 10 | | 20, 10 | | 0.2 |
| Q2 | 0.8, 15 | | | | |
| Q3 | 1.1, 20 | | | | |
| Q4 | 0.035, 2.25 | | 30, 15 | | 0.2 |
| Q5 | 0.056, 3.6 | | | | |
| Q6 | 0.077, 4.95 | | | | |
| Activation volume | $A^a$ ($s^a\mu m^a$)$^b$ | $d$ ($\mu$m) | $E^a$ (kJ/mol) | $V^a$ (cm$^3$/mol) | |
| Q7 | 0.0013, 0.03 | 1000 | 424, 335 | 6, 3 | 0.26 |
| Q8 | 0.0013, 0.03 | 10000 | 424, 335 | 6, 3 | 0.26 |

The value of $\omega$ is 1 Hz and $Q_K$ is 1000 in the upper and 10,000 in the lower-mantle for all models.
[a] First value for upper-mantle, second for lower-mantle.
[b] Value is constrained by radial seismic attenuation models.

including olivine, magnesiowüstite and perovskite analogs as well as bulk peridotite (Getting et al., 1997; Jackson, 2000; Jackson et al., 1992; Tan et al., 2001; Webb et al., 1999). The general pattern is that the frequency-dependence is quite low ($a$ between 0.1 and 0.3, consistent with the seismic observations) and does not vary significantly with temperature (Jackson, 1993; Jackson, 2000). Measurements of the activation enthalpies at various pressures (Getting et al., 1997; Karato and Jung, 2003; Tan et al., 2001; Yamazaki et al., 2000) and separate experiments to determine the peridotite solidus curve (Herzberg et al., 2000; Herzberg and Zhang, 1996; Hirschmann, 2000) provide constraints on the value of $g$. The latest experimental work on fine-grained olivine aggregates (Jackson et al., 2002 and references therein) provides parameters to model anelasticity without using additional seismic constraints. Attenuation is probably caused by a diffusion, grain-size sensitive, creep mechanism (Jackson et al., 2002; Tan et al., 2001; Webb et al., 1999). In this case, the pre-exponential factor is $B = Ad^a$, where $A$ is a scaling factor and $d$ is grain size. The activation volume has been experimentally determined for climb-controlled dislocation creep (Béjina et al., 1999).

The experimental results provide a $g$ of about 30 for olivine in the uppermost mantle (Karato, 1993), while $g = 10$–$20$ (Karato and Karki, 2001) is probably more appropriate for the lower-mantle. Higher $g$ values enhance the temperature and pressure dependence of $Q_S$. Unfortunately, no data are available for the transition zone minerals. We use values for olivine throughout the upper-mantle, and test a range of $g$ (models Q1–Q6, Table 1). Note that we fix the frequency dependence $a$ at 0.2 for all the models with the homologous temperature approach. For a frequency equal to 1 Hz, $a$ only features as a scaling factor to $g$ and it is sufficient to vary $g$. The investigated range of $g$ gives $Q_S$ models with a depth variation that is within the range of the seismic models. Uncertainties in the melting temperature (<100 °C) are negligible compared to the other uncertainties. We used the peridote solidus KLB1 (Herzberg and Zhang, 1996; Hirschmann, 2000) for the upper-mantle. We extrapolate this solidus into the shallow lower-mantle, remaining well within the upper and lower solidus bounds for the lower-mantle (Zerr et al., 1998). Note that the cusps in the attenuation models Q1–Q6 (Fig. 1) are inherited from the solidus shape. The only compositional effect included in the anelasticity was that a different solidus was used for MORB (Yasuda et al., 1994). In models Q1–Q6, $B$ was adapted (Table 1) to obtain $Q_S$ profiles for a reference mantle adiabat (with a 1300 °C potential temperature) consistent with radial seismic attenuation models. Our $Q_S$ models include a jump at the ringwoodite–perovskite transition (Fig. 1), because a steep gradient from the upper to lower-mantle is the best-constrained feature of whole mantle one-dimensional $Q_S$ profiles (Romanowicz and Durek, 2000). An additional jump in $Q_S$ at 220 km depth, often included in the parametrization of radial attenuation models, is not required because

the temperature-dependent anelasticity models already result in low attenuation in this depth range. Our synthetic models span the relatively small range of seismic $Q_S$ profiles. But, note that temperature changes of several 100 °C will introduce lateral variations in $Q_S$ on the order of 100%. Our calculations include this strong temperature dependence.

The experimental value of the activation volume for olivine (Béjina et al., 1999) is similar to estimates obtained with the relation between $H(P)$ and melting temperature. No similar data are available for the transition zone minerals. Again, we extend the olivine results to the transition zone. The new attenuation data for olivine (Jackson et al., 2002) give upper-mantle $Q_S$ values comparable with the observed seismic attenuation (Fig. 1). For perovskite and magnesiowüstite, estimates of activation enthalpies are available (Getting et al., 1997; Webb et al., 1999). We use the values for perovskite for models Q7 and Q8, since the effect of a two-phase mixture are still unexplored. Activation volumes at shallow lower-mantle pressures are determined indirectly (Yamazaki and Karato, 2001). Because the available values of $B$ are for perovskite analogs (Webb et al., 1999), the lower-mantle pre-exponential factor is again constrained by radial seismic attenuation models.

The two different approaches result in a different depth-variation of $Q_S$, both compatible with the range of seismic models. The set of attenuation models Q1–Q8 is used to assess the effect of the uncertainties in anelasticity. We will show that, in the upper-mantle, excluding anelasticity increases uncertainties in the temperature estimates more than uncertainties in the anelasticity parameters do.

### 2.3. Compositional models

To assess the influence of composition on seismic velocities and density, we consider a set of compositions: the "classical" pyrolite model for the undepleted mantle, the piclogite mantle model, which is extreme in its low olivine content, and two models representing the oceanic crust (MORB) and lithosphere (harzburgite) of the subducted slab. We also evaluate the effect of hydrous minerals in the transition zone, where they have been proposed to play a significant role (Angel et al., 2001a). All starting compositions are given in Table 2. Using these models, we implicitly investigate the effect of varying iron, silica and aluminium content, and do so in a manner that generates feasible mineral compositions. The piclogite model (Bass and Anderson, 1984) was included because with its lower magnesium and higher aluminium content, and olivine fraction of 40% against more than 60% for pyrolite, it gives us a larger range of mantle models. However, the high degree of partial melting required to form basalts from piclogite may not be geologically feasible (Jaques and Green, 1980) and various seismic models seem to favour an olivine content closer to pyrolite (Ita and Stixrude, 1992; Shearer and Flanagan, 1999). The MORB model is the classical primitive oceanic basalt composition consisting mainly of iron-rich pyroxene and garnet. The harzburgite composition is characterized by an olivine content of circa 80%.

Table 2
Starting compositions

| Mineralogy (mode, vol.%) | Pyrolite | Piclogite | Harzburgite | MORB |
|---|---|---|---|---|
| Olivine | 61.7 | 40.0 | 82.0 | – |
| CPX | 13.3 | 22.0 | – | 65.0 |
| OPX | 5.2 | 8.0 | 14.4 | – |
| Garnet | 15.3 | 22.0 | 3.6 | 25.0 |
| Jadeite | 4.5 | – | – | – |
| Ca-garnet | – | 8.0 | – | – |
| Coesite | – | – | – | 10.0 |
| FeO/MgO + FeO | 0.11 | 0.11 | 0.11 | 0.29 |

Pyrolite composition is from Irifune (1987), piclogite from Bass and Anderson (1984), harzburgite from Irifune and Ringwood (1987a), MORB from Irifune and Ringwood (1987b).

Although these compositions represent a reasonable large-scale range, it is certainly not a comprehensive set. For the inversion of seismic and gravity data, iron content is often used as sole compositional variable (Deschamps et al., 2002; Forte and Perry, 2000). In addition to using the five compositional models listed earlier, we investigate the sensitivity of seismic velocity to variations in the Fe/(Fe + Mg) ratio as well the role of Al- and Ca-bearing minerals, while keeping the rest of the mineralogy fixed. This is an often used procedure (Deschamps et al., 2001; Karato and Karki, 2001), although changes in the starting composition are also accompanied by changes in mineralogy. For example, the different mineralogy of pyrolite and piclogite (60% versus 40% of olivine) is due to slightly different proportion of aluminium, magnesium and

other elements. This is not taken into account when only the mineral Fe, Al, or Ca content is varied. Our analysis gives an estimate of the expected amplitude and sign of compositionally controlled seismic anomalies, but does not represent a full sensitivity analysis.

Summary phase diagrams are available for pyrolite and piclogite over a large range of pressure and temperature. We used the diagrams compiled by (Ita and Stixrude, 1992) which are split into one for the (Mg, Fe)$SiO_4$ component and one for the residuum. New phase equilibrium data confirm the principal features, as for instance the pressure agreement between the post-spinel transformation and seismic discontinuity at 660 km depth (Shim et al., 2000) or the negative Clapeyron slope of the same transition (Bina and Helffrich, 1994). Since the uncertainties in location of the phase boundaries and the effects of other major elements (Al, Ca) and Mg, Fe partitioning on the phase diagrams are not well known, we cannot include them in our analysis. To some extent however, the comparison of pyrolite and piclogite gives an idea about the influence of these uncertainties.

Data for the harzburgite phase diagram (Irifune and Ringwood, 1987a) are available for a narrow temperature range only. Experiments were carried out at 1300–1400 °C and up to 26 GPa. The MORB model has been taken from the work of Hirose et al. (1999), who compiled and extrapolated available phase equilibria data up to 27 GPa starting with the MORB data of Irifune and Ringwood (1987b, 1993). Because very little data is available for the probable Al-rich phase with spinel calcium–ferrite structure stable at lower-mantle condition for a MORB composition (Catti, 2001), we assume that aluminum can be stored in an exsolved Al-rich phase ($Al_2O_3$ corundum).

All of these compositions are anhydrous. However, a subducting slab can carry a relatively large amount of water into the mantle, mostly in hydrous phases (Angel et al., 2001a; Stalder and Ulmer, 2001). Also the overlying mantle wedge is likely to be hydrated by the slab (Ulmer, 2001). Even in an undepleted mantle the possibility that a certain amount of water is trapped in minerals cannot be excluded (Drake and Righter, 2002). Recent data showed that wadsleyite and ringwoodite can store a notable quantity of water (up to 3 wt.%), while above the olivine–wadsleyite transition water is probably stored in the minor alphabet phases (Angel et al., 2001a). The elastic properties of hydrous minerals reduce seismic velocities. Using elasticity data of hydrous wadsleyite and ringwoodite, we calculate the effect on seismic velocities and density in the transition zone. The wadsleyite bulk modulus and its $P$ derivative are taken from Kudoh and Inoue (1998). The density of hydrous wadsleyite and $\rho$, $K_S$ and $G$ of hydrous ringwoodite are from Inoue et al. (1998), and $\partial K_S/\partial P$ for hydrous ringwoodite is from Yusa et al. (2000). Other values are not modified from the respective anhydrous phases. The used data are for samples with circa 2 wt.% of water content. Slab water content is more likely to be below 1 wt.% (Angel et al., 2001a). A decrease of the melting temperature (Litasov et al., 2001), will lower $Q_S$ and cause a further reduction of the seismic wave velocities (Karato and Jung, 1998) but is not included here.

## 3. Synthetic seismic velocities: uncertainties and sensitivity

Our method supplies $V_P$, $V_S$ and density for a given mineralogical model as function of pressure and temperature. The conversion from pressure to depth is done using the pressure profile of PREM (Dziewonski and Anderson, 1981). We first take a look at how uncertainties in the mineral physics parameters (Table A.1 and models Q1–Q8) affect predicted seismic parameters. Subsequently, we investigate the sensitivity of the seismic velocities and density to temperature and composition throughout the upper-mantle. These results give an indication of the feasibility of interpreting or inverting seismic models for temperature and/or compositional variations.

### 3.1. Uncertainties in forward calculation

In Fig. 2 (left panels) we plot the $V_P$, $V_S$ and density pattern for dry pyrolite as a function of pressure and temperature. Obvious sharp gradients result from the phase transitions of olivine to wadsleyite and ringwoodite to perovskite and are related to the seismic 410 and 660 km discontinuities. The enhanced effect of anelasticity on approach of the melting temperature is responsible for the non-linear variation of velocities with temperature. At a given depth (and composition) each velocity corresponds uniquely to one temperature. The diagrams in Fig. 2 can thus be

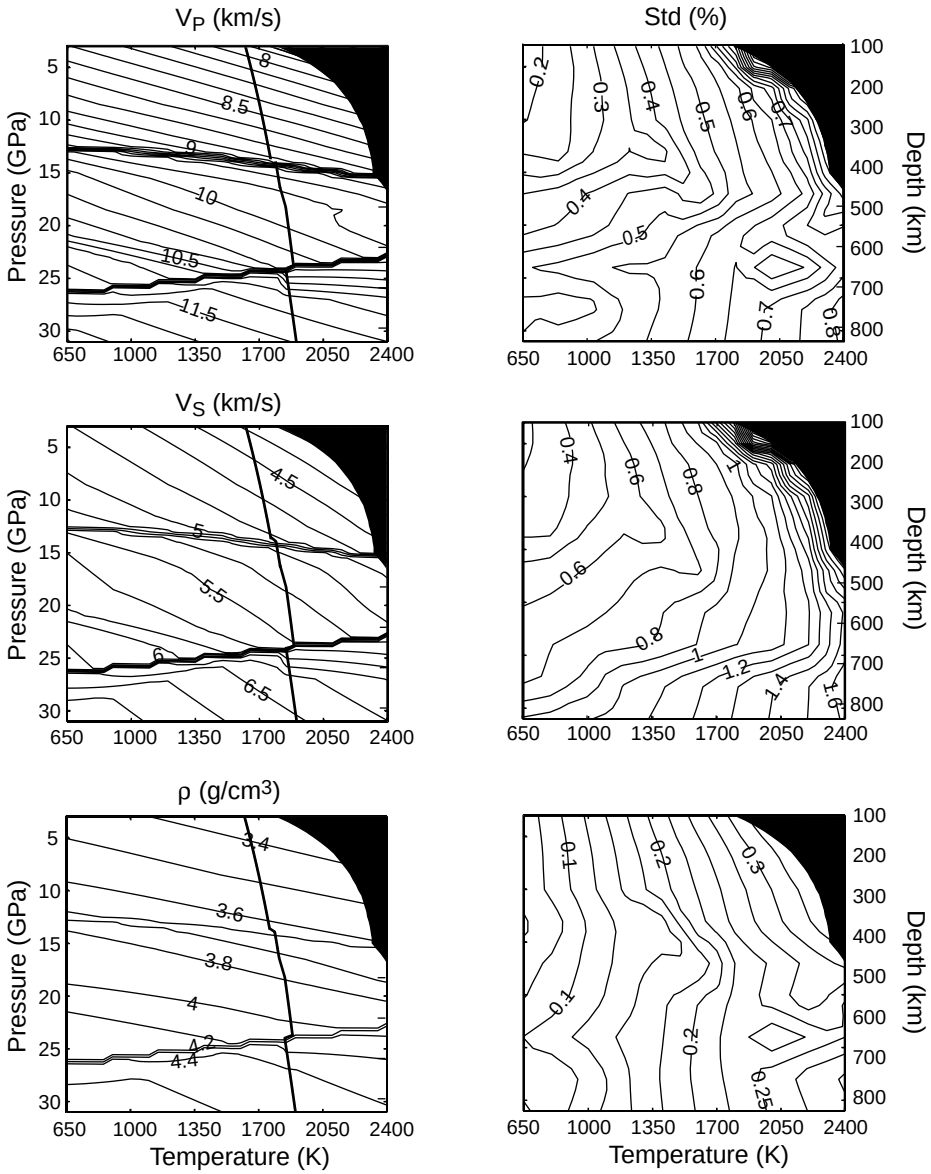


Fig. 2. Seismic wave velocities ($V_P$ and $V_S$) and density ($\rho$) for dry pyrolite as a function of pressure ($P$) (or depth) and temperature ($T$). The bold line corresponds to a mantle adiabat with a potential temperature of 1300 °C. The area above the dry solidus has been masked in black. The uncertainties in the seismic properties resulting from uncertainties in the anharmonic and anelastic parameters are shown as standard deviations in the panels on the right.

used for a rapid temperature estimate when seismic velocities and depth are known. For example, if we have a P-wave velocity of 8.5 km/s at 300 km depth, the inferred temperature will be 1855 K if the composition is dry pyrolite. Note that absolute velocities are necessary for inferring temperature because of the non-linear dependence on temperature. From the results of the forward calculation of $V_P$ and $V_S$ from temperature (Fig. 2), it can be inferred that small variations in velocities (e.g. circa 0.5% in $V_P$ and 0.8%

in $V_S$ at 300 km) correspond to large temperature variations (circa 5%).

Randomly varying the elastic and anelastic parameters within their uncertainty bounds results in a range of seismic velocities and density. The velocity and density estimates are well approximated by a normal distribution, and the resulting uncertainties for $V_P$, $V_S$ and density are reported in Fig. 2 (right panels) as standard deviations ($\sigma$) in percent. Overall, uncertainties increase with temperature and pressure. Density uncertainties are the lowest, not quite reaching 0.4%, and are not strongly affected by the large uncertainties in $\alpha$. The $\sigma$ variations of $V_S$ reach a maximum value of 1.6% and are almost double $\sigma(V_P)$. This is due to the poorer constraints on shear than bulk modulus parameters. Note that uncertainties in m/s are similar in size for $V_P$ and $V_S$, since $V_P$ is close to a factor two higher than $V_S$. Finally, uncertainties in both velocities show a high gradient close to the solidus. This is because changes in anelasticity parameters have the largest effect close to the solidus.

### 3.2. Temperature sensitivity

To illustrate how velocities and density change in response to variations in temperature, we calculate temperature derivatives for $V_P$, $V_S$, bulk sound velocity ($V_\phi$), $\rho$ and their uncertainties. Anelasticity makes the temperature derivatives of $V_P$ and $V_S$ strongly temperature-dependent and increases their uncertainties. In many applications, a constant or depth-dependent factor is used to scale seismic velocity anomalies to temperature, thus ignoring this temperature dependence. In fact, where anelasticity is important, absolute velocities are necessary to infer temperatures.

To isolate pure temperature sensitivity we keep phase-transition depths fixed over the differentation interval of $\pm 1\,^\circ$C. Allowing phase-transition depths to shift with temperature introduces strong, but confined peaks around the sharp discontinuities. The temperature derivatives are very similar for different compositional models, therefore, only the results for pyrolite are shown (Fig. 3). We plot the derivatives for three different adiabats, with potential temperatures of 1000, 1300, and 1600 °C, that cover the range of temperature expected in different geodynamic environments. The 1300 °C adiabat is a typical mantle reference adiabat, while a 1000 °C adiabat may be representative of subduction zones and a 1600 °C adiabat can be adopted as a likely thermal regime for upwelling plumes. Uncertainties are calculated for the derivatives along the 1300 °C adiabat, using the same procedure as in the previous section (Fig. 3). Due to the exponential temperature dependence of anelasticity, uncertainties are larger at higher temperature and smaller at lower temperature, with anharmonic uncertainties as a lower bound.

Overall, absolute values of the temperature derivatives decrease with increasing pressure and decreasing temperature. Density and $V_\phi$ derivatives (Fig. 3c and d) are a factor two to five smaller than $V_P$ and $V_S$ derivatives (note the different scales in the different panels in Fig. 3). The small differences in $\partial \ln V_\phi/\partial T$ and $\partial \ln \rho/\partial T$ and the anharmonic parts of $\partial \ln V_P/\partial T$ and $\partial \ln V_S/\partial T$ along the different adiabats are due to the changes in mineral assemblage for a pyrolitic composition at varying $P$–$T$ conditions. For instance, the olivine–wadsleyite transition becomes deeper and the ringwoodite–perovskite shallower at increasing temperature due to the Clapeyron slopes. A decrease of the sensitivity of velocity to temperature characterizes the stability field of wadsleyite (depth range around 400–520 km). Below the wadsleyite–ringwoodite transition (~520 km depth) sensitivity increases again (Fig. 3) followed by a decrease below the ringwoodite–perovskite transition (~660 km) for $V_P$ and $V_S$ as well as for $V_\phi$. These variations are due to the different $\partial \ln K_S/\partial T$ and $\partial \ln G/\partial T$ for the different high-pressure phases of olivine and are a robust feature in spite of the large uncertainties in these parameters. The effect of the decrease of $|\partial \ln K_S/\partial T|$ of perovskite + magnesiowüstite relative to ringwoodite + majorite is reduced in the $V_P$ anharmonic temperature derivatives by the opposite behaviour of the shear modulus. For density, a decrease in the temperature derivatives is observed in the ringwoodite stability field.

The anharmonic part of $\partial \ln V_P/\partial T$ and $\partial \ln V_S/\partial T$ is almost constant with temperature where composition and phase do not change. Anelasticity introduces a strongly non-linear dependence on temperature resulting in a large increase of $|\partial \ln V_{P,S}/\partial T|$ with increasing temperature. For example, a 1% anomaly of $V_S$ at 200 km depth will convert into a $\Delta T$ of 125 K along the 1000 °C adiabat, 80 K along the 1300 °C

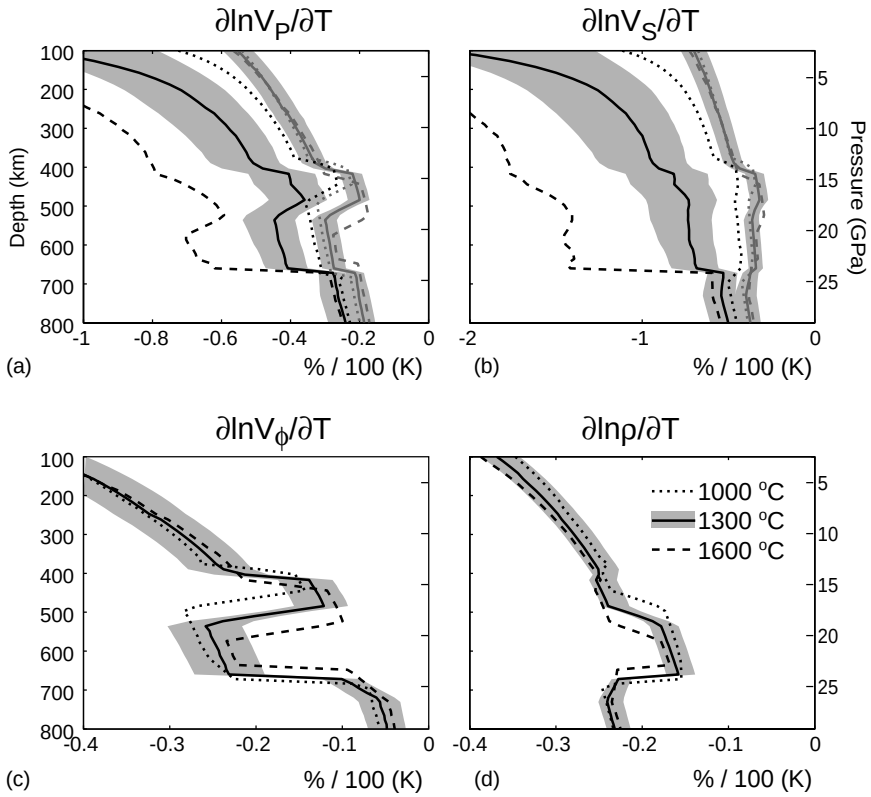


Fig. 3. Temperature derivatives of $V_P$, $V_S$, bulk sound velocity ($V_\phi$) and $\rho$ are shown as a function of depth. Dotted, solid and dashed lines are for 1000, 1300 and 1600 °C adiabats, respectively; gray lines correspond to purely anharmonic derivatives. Light gray fields illustrate uncertainties in anharmonic and full derivatives along the 1300 °C adiabat. Anelasticity (model Q5 is applied) makes the derivatives of the seismic wave velocities temperature dependent (black lines) and significantly increases temperature sensitivity in the upper-mantle.

adiabat and 45 K along the 1600 °C adiabat (Fig. 3). Thus, positive and negative velocity anomalies (e.g. subducting slab and plume anomalies) of the same amplitude translate into temperature anomalies with different amplitudes. Again, this emphasizes that where anelasticity plays a significant role, absolute velocities are required for a thermal interpretation. The total $V_S$ derivatives, with anelasticity included, are about twice those for $V_P$. For the reference 1300 °C adiabat, $\partial \ln V_S/\partial T$ is $-2.1\%/100$ K at 100 km depth reducing to $-0.7\%/100$ K at the base of the transition zone. Uncertainties in the derivative values are large (Fig. 3) and for a $g$ of 30 encompass the derivative values for $\pm 200$ °C. But the difference between derivatives with and without anelasticity is significant throughout the upper-mantle. Thus, it is important to include the non-linear temperature dependence of $\partial \ln V_{P,S}/\partial T$ for temperature variations larger than about 200 °C. The effect of anelasticity decreases not only with decreasing temperature, but also with increasing depth. In the lower-mantle, anelasticity contributes only about 20% of $\partial \ln V_{P,S}/\partial T$, and the difference with the anharmonic derivatives is barely to not significant, consistent with the results of (Trampert et al., 2001). If a strong jump in $Q_S$ is included, the derivatives below the 660 km discontinuity are influenced principally by anharmonic effects. If the increase in $Q_S$ around 660 occurs more gradually, anelasticity may still be important in the shallow lower-mantle while losing its importance deeper.

For the bulk sound velocity (Fig. 3c), we do not plot anharmonic derivatives, since they are almost equivalent to the derivatives including anelasticity, due to the high constant bulk attenuation used. Bulk

sound derivatives are comparable in magnitude to those for density, around −0.35%/100 K at 200 km depth and −0.25%/100 K at 400 km depth. Below the ringwoodite–perovskite transition, the temperature sensitivity of $V_\phi$ reduces drastically, $\partial \ln V_\phi/\partial T$ lowers to a value of about −0.12%/100 K. The obvious advantage in using bulk sound velocities for the interpretation of global models is to avoid the use of the less well-constrained shear moduli of the mantle minerals and the uncertainties due to the anelasticity parameters. This consideration lead many authors (Ita and Stixrude, 1992; Jackson and Ridgen, 1998; Lithgow-Bertelloni, 2001) to use $V_\phi$. On the other hand, $V_\phi$ models are often reconstructed starting from separate $V_P$ and $V_S$ models. Also in a joint inversion of $V_P$ and $V_S$ (Kennett et al., 1998; Masters et al., 2000; Su and Dziewonski, 1997; Vasco and Johnson, 1998), the different propagation and coverage of the P- and S-waves may influence the final result. Finally, the low temperature sensitivity of $V_\phi$ means that bulk sound velocity needs to be resolved significantly better than $V_P$ and $V_S$ if thermal structure is to be inferred.

### 3.3. Compositional sensitivity

As discussed earlier, no single parameter describes the effect of variations in upper-mantle composition. Instead of calculating derivatives, the expected amplitude of upper-mantle velocity and density anomalies due to compositional variations is assessed by calculating the difference with pyrolite seismic parameters for all assemblages discussed in Section 2.3 (Fig. 4). In addition, the sensitivity to variations of single major chemical elements (Fe, Al, Ca) without changing mineralogy is addressed below. Note that in Fig. 4 the same scale is used for each panel, in contrast to Fig. 3, in which the density and $V_\phi$ scales were 10 times smaller than the $V_P$ and $V_S$ scales.

The velocity and density differences between the more accepted pyrolite model and the more extreme piclogite model do not exceed 1% (Fig. 4), confirming the seismic similarity already found in previous studies (Ita and Stixrude, 1992; Nolet and Zielhuis, 1994; Vacher et al., 1998). The two undepleted mantle models comprise an extreme range of average upper-mantle compositions, being especially different in terms of Si/(Si + Mg) ratio. The velocity differences are small for what is generally resolvable in upper-mantle tomography and significantly less than expected for variations of several hundred degrees in temperature. Piclogite has smaller jumps at 410 and 660 km depth than pyrolite and a higher gradient throughout the transition zone, resulting in sign changes of the difference. These characteristics have sometimes been used as argument for a piclogitic composition (Bass and Anderson, 1984; Duffy et al., 1995), but seismically the jumps are not well constrained (Shearer, 2000) and pyrolite can also give an acceptable fit (Gaherty et al., 1999b). In bulk sound velocity, the 660 km jump and the gradient are less pronounced and the difference between piclogite and pyrolite is small as well.

The slab compositions have a different signature as a function of depth than pyrolite (Fig. 4). The differences between undepleted mantle and the lithospheric part of the slab (harzburgite) are mostly less than 0.5% in velocity, except just above 400 km where garnet, which is a more important component in pyrolite, starts transforming. Along the same adiabatic geotherm, the densities are 2% lower than pyrolite above 400 km. This will offset some of the negative buoyancy that results from the lower subducting slab temperatures.

The differences between the undepleted mantle and the crustal part of the slab are the largest both for velocities and density, reaching values of up to 4% in velocity above 400 km, and in $\rho$ in the transition zone (Fig. 4). The mineralogical discontinuities are associated with steep gradients and sometimes sign changes. Despite the strong contrast between MORB and pyrolite seismic properties, the small thickness of the crustal part of the slab may make it difficult to seismically detect the velocity variations. Also, the geodynamic role of the negative density contrast of oceanic crust around 660 km depth, both with pyrolite and harzburgite, is not clear. Perhaps the fate of the subducted crust is linked to the underlying lithosphere (Gaherty and Hager, 1994) or it may form a separate layer in proximity of the 660 km discontinuity (Hirose et al., 1999; Karato, 1997). Only if such separation occurs and significant amounts of crust accumulate would it have a signature in most tomographic models.

Additional calculations varied only Fe-, Al-, or Ca-content. A 4% decrease in the Fe-content of pyrolite (from Mg# 89 to 93) gives an increase of $V_S$ of 1%, $V_P$ of 0.7% and $V_\phi$ of 0.5% (Fig. 4). The

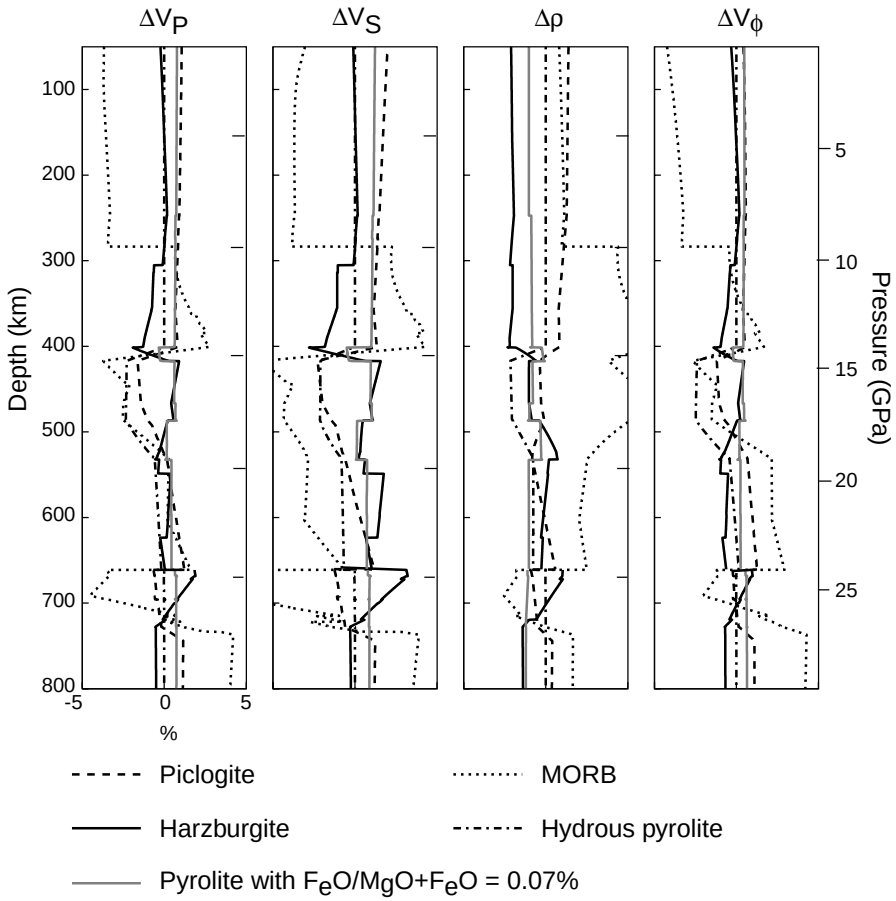


Fig. 4. Seismic velocity and density anomalies relative to pyrolite for various compositions as a function of depth along a 1300 °C adiabat. Hydrous pyrolite is only considered in the transition zone using data for hydrous wadsleyite and ringwoodite. Compositional variations have a similar amplitude for all seismic parameters. In some cases, density and/or bulk sound velocity show opposite behaviour from $V_P$ and $V_S$.

effect on density is a decrease of 1%. It should be noted that, although some more extreme compositions are found, the majority of xenoliths and mantle peridotites have magnesium numbers between 88 and 92 (see e.g. McDonough and Sun, 1995). If these samples are representative for the composition of the upper-mantle, variations in iron content have a small seismic effect compared to potential thermal variations. Deschamps et al. (2002) inferred variations of up to 3% in iron content in a joint inversion of $V_S$ and density that maps all non-thermal variations into iron content. This is on the high end of the mantle sample range. Changes in Al-content (present in the garnet phase) and Ca-content (in garnet and Ca-pyroxene) have only a small effect on seismic velocities, due to the low volume percentages of the involved minerals. For example, substituting 1% of garnet by Ca-garnet in the total volume will increase, in the transition zone, $V_S$, $V_P$, and $V_\phi$ by 0.1, 0.05 and 0.01%, respectively, and reduce density by 0.01%. A similar small effect results from changing garnet to a more majoritic (Al-rich) solid solution in the upper-mantle, as can be seen directly from the parameters in Table A.1. Aluminum may significantly alter the physical properties of perovskite (Weidner and Wang, 1998) in the shallow lower-mantle (below 30 GPa) where sufficient oxygen vacancies exist for the anomalous incorporation of aluminum into the structure (Oganov and

Brodholt, 2000). We stress again that the analysis performed is only indicative. For instance, we did not include the unknown effects of variations in chemical composition on phase diagrams, which may, at least locally near the phase transition boundaries, introduce large anomalies.

Finally, the effect of the different elasticity of the hydrous transition zone minerals with 2 wt.% water is a strong decrease of 3.5% in $V_\phi$, $V_P$ and $V_S$ with respect to pyrolite. Density also shows a small decrease. Note that there are only few data, especially for the shear modulus. The additional anelasticity effect due to a cooler solidus (Litasov et al., 2001) may enhance the velocity reduction. If the water content were only 1 wt.%, which may be more plausible (Angel et al., 2001a), the effect would be only about half that shown. We do not test the effect of water above the 410 km discontinuity because of the unknown properties of the alphabet phases, which probably store water above the transition zone (Angel et al., 2001a). However, the volume fraction of these phases is probably too small to significantly affect large-scale velocities.

A general feature emerging is the independent behaviour of the density and seismic velocities. In particular, both seismic velocities may vary strongly, while the density remains essentially unchanged (for example for MORB). This feature indicates the failure of Birch's law which assumes linearity between velocities and density (Karki et al., 2001). This opposite behaviour is exploited in combined inversions of density and velocity to separate thermal and non-thermal effects (Deschamps et al., 2002; Forte and Perry, 2000).

## 4. Feasibility of interpreting upper-mantle seismic velocities

Using the uncertainties and sensitivities discussed in Section 3, we evaluate the feasibility of interpreting upper-mantle seismic models in terms of temperature and composition. In the upper-mantle, seismic velocities are most sensitive to temperature. However, as the sensitivity to temperature decreases with depth, the sensitivity to variations in compositions becomes more important. While keeping in mind possible trade-offs with compositional structure, it may be useful to, as a first approximation, or as end-member interpretation, perform a purely thermal interpretation. Below, we first discuss the uncertainties in temperatures that would be obtained in an inversion for thermal structure only, assuming that seismic velocities are well constrained and composition and depth are known. The sensitivity analyses also show that, where anelasticity plays a significant role (i.e. in most of the upper-mantle), one can only interpret absolute velocities, not velocity anomalies. Seismic models are often presented in terms of anomalies relative to a reference model. In many cases, the model of seismic anomalies is not very dependent on the one-dimensional background structure, i.e. absolute velocities are not well constrained. To illustrate the effect a one-dimensional background model can have on the interpretation, we perform a purely thermal interpretation of several commonly used spherically symmetric models. Finally, an investigation of heterogeneity ratios, which summarize the difference in sensitivity of $V_P$, $V_S$, density and $V_\phi$ to temperature or composition, illustrates what can or cannot be gained from joint inversions for various seismic parameters.

### 4.1. Inversion for temperature

To quantify how well mantle temperatures can be determined from a given absolute seismic velocity model, assuming a fixed composition, we follow the same statistical procedure as in Section 3.1, but for a fixed $V_P$ or $V_S$. We use the pyrolitic composition and again run 2200 random calculations for each point. The values of $V_P$ and $V_S$ are chosen so as to obtain temperature uncertainties over the range of $P$ and $T$ conditions appropriate for the upper- and shallow lower-mantle. The temperature uncertainties for a given $V_P$ and $V_S$, are similar, therefore we discuss only one pattern. The standard deviations calculated from $V_P$ are shown in Fig. 5.

The uncertainties in temperature increase with pressure and temperature and give a range of approximately $\pm 75$ K around 300 km. The uncertainties become larger in the transition zone. When crossing sharp phase transitions (i.e. the olivine–wadsleyite or ringwoodite–perovskite + magnesiowustite), temperature distributions become non-normal. In these areas we do not plot the temperature uncertainties. This trade-off between the (often not well constrained) phase transition depths and temperature makes it difficult to interpret seismic velocities in terms of

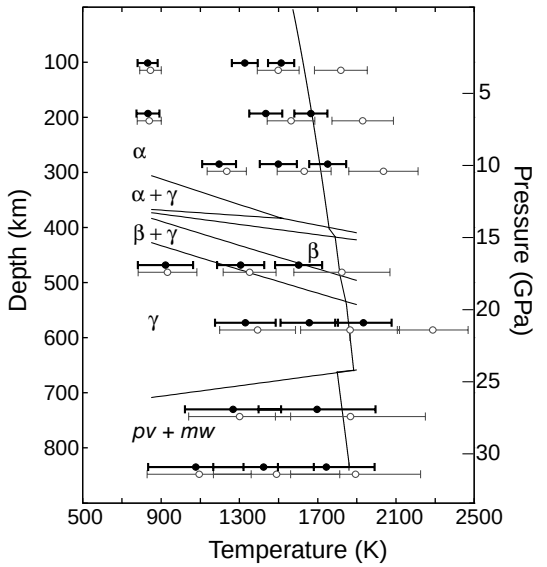


Fig. 5. Mean and standard deviations of temperature estimates for a given $V_P$ and depth taking into account uncertainties in anharmonic and anelastic parameters. White circles and thin lines show temperature estimates when only anharmonic effects are considered. (•) and (▬) illustrate the temperatures obtained when anelastic effects are included. For reference, thin lines mark the olivine phase transitions, and a mantle adiabat with a potential temperature of 1300 °C is plotted as bold line.

temperature nearby sharp phase transitions. But if the transitions are broad, as in the case of the wadsleyite to ringwoodite transformation, the distributions are still close to Gaussian. In the shallow lower-mantle, the temperature uncertainties reach values around ±250 °C (Fig. 5). The temperature uncertainties do not increase when the effect of anelasticity is included, but in the upper-mantle the mean values of the temperature distributions are significantly reduced. Seismic velocities are not strongly sensitive to variations in $Q_S$. A variation of 50% of $Q_S$ will decrease $V_P$ or $V_S$ by about 0.3%. However, if anelasticity is not included, implying a $Q_S$ equal to infinity, seismic velocities are significantly higher. In the lower-mantle, the higher values of $Q_S$ make anelasticity a less important factor.

### 4.2. Absolute velocities—one-dimensional reference models

To compare various global one-dimensional models, which form the background or starting model for most other seismic models, a purely thermal interpretation of these models was made. We set out to gain a better understanding of the average thermal structure of the upper-mantle. However, it turns out that non-uniqueness of the one-dimensional models complicates a detailed interpretation, and the analysis instead documents the limitations on interpreting current one-dimensional reference models. The models we interpret are the most commonly used global one-dimensional models AK135 (Kennett et al., 1995) and PREM (Dziewonski and Anderson, 1981) as well as PEM-C and PEM-O (Dziewonski et al., 1975). It is useful to keep in mind that the models are influenced by the distribution and type of data, as well as by the parameterization used.

#### 4.2.1. One-dimensional global seismic models

The AK135 model (Kennett et al., 1995) is based on the body-wave travel times from the ISC catalogue. It is a relatively high frequency model (∼1 Hz) and P-wave velocity is better constrained than S-wave velocity. The AK135 density model has been obtained by inverting the body-wave data to also fit normal mode observations (Montagner and Kennett, 1996). The non-uniform geographic coverage of the seismic stations biases the AK135 model to continent and subduction zone structure.

The PREM model (Dziewonski and Anderson, 1981) is constructed using free-oscillations, surface-wave phase velocities and travel times of body-waves. The lower frequency normal modes and surface waves (0.3 and 15 mHz) provide the main constraints for S-velocity. The body-wave data improve the resolution of P-wave velocities. The normal modes and phase velocity data also provide constraints on density and attenuation structure of the Earth. However, these constraints are not sufficient to fully resolve density structure. In addition, PREM density was required to satisfy Birch's law in the upper-mantle, and lower-mantle densities were assumed to be consistent with the adiabatic compression of a homogeneous layer. PREM includes a strong discontinuity at 220 km depth as well as transverse anisotropy above this depth. The presence of anisotropy is also found in other studies (e.g. Laske and Masters, 1998; Montagner, 1998; Montagner and Tanimoto, 1990), but a global isotropic discontinuity at 220 km depth is not consistent with more recent work (e.g. Revenaugh

and Jordan, 1991) and not necessary to obtain a satisfactory fit of the data (Laske et al., 2001; Ritsema and van Heijst, 2001).

Regional studies yield evidence of lateral heterogeneity of the upper-mantle. The two models PEM-O and PEM-C (Dziewonski et al., 1975), predecessors of PREM, differentiate between upper-mantle velocities under continental and oceans regions on the basis of free-oscillation data. The 220 km discontinuity was already included in PEM-O, while PEM-C is characterised by a higher velocity gradient around this depth. Below 400 km depth the two PEM models are the same.

*4.2.2. Interpreting one-dimensional models*

As found in previous studies (Ita and Stixrude, 1992; Jackson and Ridgen, 1998; Vacher et al., 1998; Weidner, 1985) a pyrolitic mineralogical model along a 1300 °C adiabat provides a reasonable first-order fit to the global seismic models (Fig. 6). Nevertheless, some discrepancies, such as the higher pyrolitic velocity jump at 410 km depth, a different velocity gradient in the transition zone, and larger discontinuities at 410 and 660 km have been consistently found and remain also with the latest elasticity and anelasticity data. Seismic profiles for a 150 K higher adiabat are shown for piclogite, because of the high degree of partial melting required to form mid-ocean-ridge basalts from a piclogitic source (Jaques and Green, 1980). The difference between a pyrolitic and piclogitic model is less than the difference between the global seismic models. Note that the purely oceanic model PEM-O resembles the mineralogical models most closely (Fig. 6).

In Fig. 7 we present the temperature estimates $T_P$ and $T_S$ obtained when $V_P$ and $V_S$ are inverted assuming a pyrolitic composition. The results from the purely thermal interpretation do not look very useful. First of all, the temperature profiles fluctuate wildly around the adiabat, and negative temperature gradients occur in several depth ranges. Second, the small velocity differences between the global models translate into large disparities in inferred temperature. Third, *P* and *S* models yield incompatible temperature estimates especially in the transition zone. Two possible causes for the failure of a thermal interpretation of the reference models can be identified: (1) uncertainties in the seismic models; (2) non-thermal physical structure.

Seismic models are always non-unique (e.g. (Montagner and Kennett, 1996; Paulssen, 1988). For

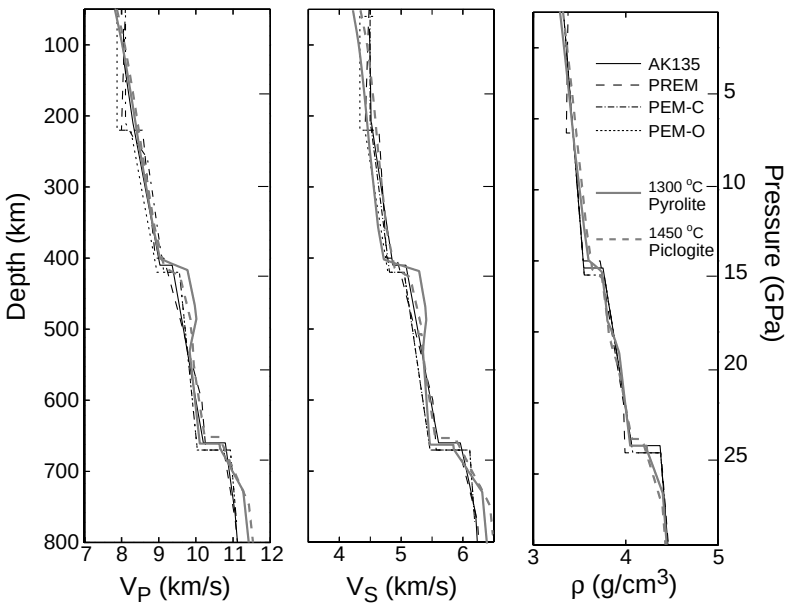


Fig. 6. Seismic velocities and density calculated for a pyrolitic mantle following a 1300 °C adiabat and a piclogitic mantle following a 1450 °C adiabat are to a first-order consistent with four global seismic one-dimensional models.

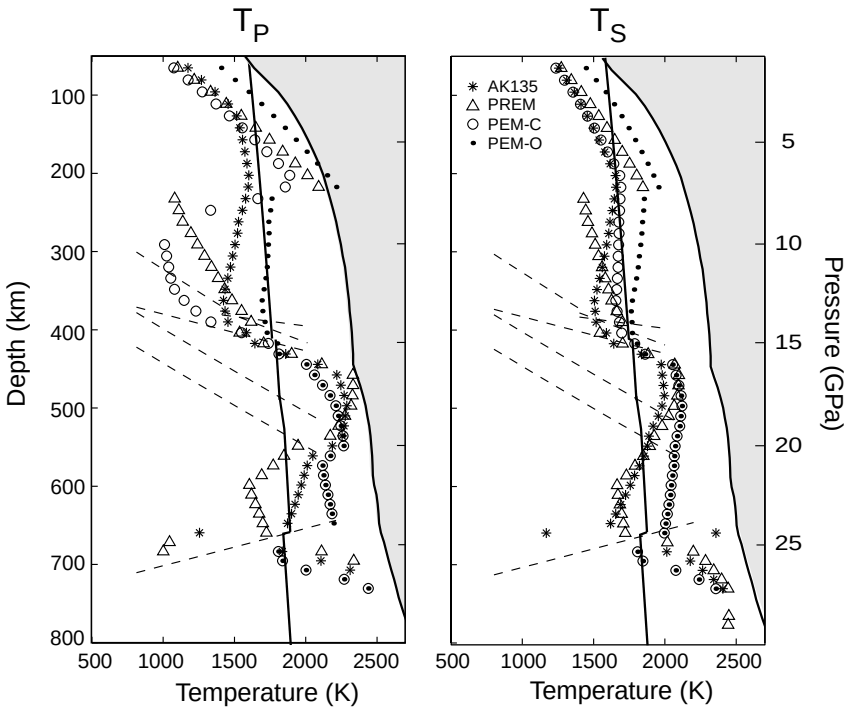


Fig. 7. Purely thermal interpretation of $V_P$ and $V_S$ of PREM (△), AK135 (✳), PEM-C (○) and PEM-O (●), assuming a pyrolitic mantle. Dashed lines correspond to olivine phase-transitions, the solid line is a 1300 °C adiabat. The gray field marks the region above the dry solidus. Note that small (and possibly not resolved) differences in absolute velocity models can translate into large temperature differences.

instance, the 220 km seismic discontinuity and the preceding negative seismic gradient have been included a priori in the PREM and PEM models (Dziewonski and Anderson, 1981; Dziewonski et al., 1975), but they are not required by the seismic data (Laske et al., 2001; Ritsema and van Heijst, 2001). The jump at 220 km depth included in the PREM and PEM models cannot be translated into thermal structure.

The smaller seismic jump at 410 and 660 km depth than predicted by an adiabatic pyrolite model, translate into very high temperatures below both transitions. Lithgow-Bertelloni (2001) also retrieved high transition zone temperatures from bulk sound velocities and argued for possible melt occurrence there. The different temperatures in the transition zone obtained from $V_P$ and $V_S$ do imply non-thermal effects. For example, the presence of hydrous minerals in the transition zone could play a role. However, the negative temperature gradient below 410 brings temperatures back to the mantle adiabat. Instead, the amplitude of 410 km and 660 km velocity jumps may be underestimated in the global seismic models, and by different amounts for $V_P$ and $V_S$ (Shearer, 2000). Depending on the frequency content, the seismic data may only sample part of the phase transition which occurs non-linearly over a finite depth range (Gaherty et al., 1999b; Stixrude, 1997). A stronger 410 velocity jump and lower transition zone gradient, similar to those predicted by an adiabatic model, may be able to yield similar average velocities and also satisfy the seismic data. While these uncertainties are unresolved, a thermal interpretation of transition zone velocities is difficult.

Only a few features of the retrieved temperatures above 400 km appear to correspond to physical structure. $T_P$ and $T_S$ from AK135 (that does not contain a 220 discontinuity) are compatible with a lithosphere with a high thermal gradient and an adiabatic temperature profile below. However, the adiabat is significantly colder than $T_{pot} = 1300\,^{\circ}C$, possibly a reflection of the continent-subduction zone bias of AK135. Presumably, oceanic mantle structure is closest to that of a thermally convecting mantle. Indeed,

the PEM-O model follows the 1300 °C mantle adiabat below 300 km, and is significantly warmer than all other models. In contrast, PEM-C temperatures are quite far from adiabatic. The very different $T_P$ and $T_S$ of PEM-C may, in part, reflect a compositional and/or anisotropic signature in subcontinental velocities (Jordan, 1988).

The one-dimensional global models represent an average of the laterally heterogeneous Earth structure. Because seismic velocities, density and anelasticity depend non-linearly on temperature, average seismic structure does not necessarily translate into average thermal structure. Therefore, regional models that average over areas with a similar tectonic structure are better suited for thermal interpretation. PEM-O and PEM-C distinguish between mantle structure beneath oceans and continents. These two models are however, also affected by large averaging effects. Many one-dimensional regional models have been produced for different tectonic regions using various data sets and processing techniques (e.g. Gaherty et al., 1999a; Gudmundsson and Sambridge, 1998; Kato and Nakanishi, 2000; Nolet et al., 1994; Paulssen, 1988). Several of these models were converted to temperature. However, we found that despite the more appropriate assumption of one-dimensional structure for smaller regions, the thermal interpretation of regional models shows essentially the same features as for the global models. For many regional models the inversions are, in fact, damped towards a one-dimensional global model. Furthermore, parametrization is often similarly coarse and resolution may not allow constraining velocities tighter than the averaged global models. The differences between continental and oceanic regions documented by the PEM models are confirmed by the regional studies.

In summary, the physical interpretation of global one-dimensional models will affect the interpretation of most seismic models in one-, two- and three-dimensional. Further work is necessary to find out whether average structure deviates from a pyrolitic mantle with an adiabatic temperature profile.

### 4.3. Separating thermal and compositional effects

So far we have concentrated on recovering constraints on mantle temperature from seismic models. Ultimately, one would also like to constrain possible compositional structure. The different seismic velocities and density have disparate sensitivities to temperature and composition. For the interpretation of seismic structure it may thus be useful to combine more that one parameter and an increasing number of studies performs joint inversions for $V_P$ and $V_S$, $V_\phi$ and $V_S$, or $V_S$ and density (Ishii and Tromp, 1999; Kennett et al., 1998; Masters et al., 2000; Su and Dziewonski, 1997; Vasco and Johnson, 1998). The seismic heterogeneity ratios, $R_{S/P} = \partial \ln V_S / \partial \ln V_P$, $R_{\phi/S} = \partial \ln V_\phi / \partial \ln V_S$, $R_{\rho/P,S} = \partial \ln \rho / \partial \ln V_{P,S}$, have been used to investigate the physical cause of seismic velocity and density anomalies (Karato and Karki, 2001; Kennett et al., 1998; Saltzer et al., 2001). Some caution has to be exercised because (1) these ratios are expected to vary significantly with temperature and (2) the seismically mapped ratios depend on the background model, where, as was shown above, the reference model for the different parameters, e.g. $V_P$ and $V_S$, may actually not correspond to the same physical conditions.

Here we investigate on the end-member (thermal or compositional) ratios. Our calculations give an expected range of $\partial \ln V_S / \partial \ln V_P$ for thermal variations ($R^T_{SP}$) from 1.3 (for low temperature, where the effect of the anelasticity is weak) to 2.2 (at high temperature, with a strong anelasticity effect) in the upper-mantle (Fig. 8a). $R^T_{SP}$ stays constant with depth in the first 400 km if temperature follows an adiabat. In the transition zone, the ratios increase at the olivine–wadsleyite phase transition and decrease at the wadsleyite–ringwoodite transition. Below the 660 km discontinuity, the increase of $Q_S$ causes the reduction of temperature effects resulting in a ratio that is almost constant around a value of 2. As with the temperature derivatives, the uncertainties in the ratios increase with temperature. Anelasticity introduces significant variation of $R^T_{SP}$ in the whole upper-mantle, while in the lower-mantle the effect of anelasticity is negligible (Fig. 8a).

The thermal $\partial \ln V_\phi / \partial \ln V_S$ ratio (Fig. 8b) shows similar features with depth and temperature as $R^T_{SP}$. Note however, that $R^T_{\phi/S}$ is defined with $V_S$ in the denominator. A range of 0.1 (high temperature) to 0.7 (low temperature) is calculated for thermal $R^T_{\phi/S}$ in the upper-mantle. The values first decrease and then increase in the transition zone. The $\partial \ln \rho / \partial \ln V_S$ ratio, $R^T_{\rho/S}$, (Fig. 8c) has a temperature dependent range of 0.15–0.5 in the upper-mantle and a value around 0.45

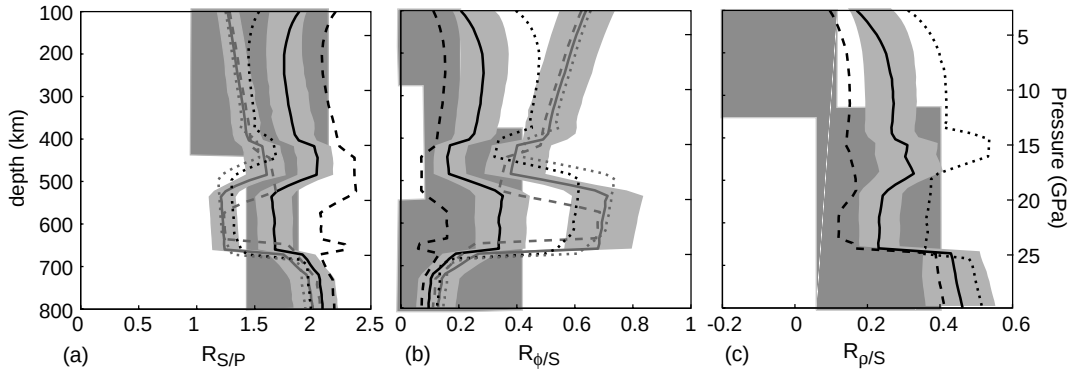


Fig. 8. Thermal heterogeneity ratios $R_{S/P}$, $R_{\phi/S}$, $R_{\phi/S}$ calculated for dry pyrolite are compared with a range observed ratios. Dotted, solid and dashed lines are for 1000, 1300 and 1600 °C adiabats, respectively; gray lines correspond to the purely anharmonic ratios. Light gray fields illustrate uncertainties in anharmonic and full ratios along the 1300 °C adiabat. Dark gray fields for $R_{S/P}$, $R_{\rho/S}$ illustrate the range obtained from seismological observations and the range of $R_{\rho/S}$ inferred from geoid data and seismic models (discussion and references in the text). In most of the upper-mantle, observed heterogeneity ratios fall within the predicted thermal range.

in the shallow lower-mantle. In this case, the transition zone is characterized by an increase of the ratio below the 410 km discontinuity, followed by a decrease until the base of the transition zone. A further sharp increase is observed below the 660 km, again due to the lower-mantle anelasticity model used.

A comparison of the variations shown in Fig. 4 gives an indication of the expected range of compositional heterogeneity ratios. For example, in the transition zone, MORB has a faster $V_\phi$ compared to pyrolite and a slower $V_S$, while harzburgite shows the opposite pattern (Fig. 4). This results in a negative compositional $R^C_{\phi/S}$ in the deep transition zone for both slab components. In the upper 400 km, the sign of $V_S$ and $V_\phi$ changes is always the same and never leads to negative $\partial \ln V_\phi / \partial \ln V_S$. Moreover, it is difficult to obtain a negative compositional ratio of $\partial \ln V_P / \partial \ln V_S$ even in the transition zone, due to the influence of the shear modulus on $V_P$.

A compositional change from pyrolite to MORB gives $R^C_{S/P}$ and $R^C_{\phi/S}$ close to 1 in the shallow upper and lower-mantle, which is lower than expected thermal ratios. In most of the upper-mantle, $R^C_{\rho/S}$ for MORB is negative, except around 300–400 km, where values are 1 to 2. All upper-mantle $R^C_{\rho/S}$ values for MORB are outside of the thermal range, but shallow lower-mantle values are not. Similary to MORB, harzburgite $R^C_{\rho/S}$ in the upper-mantle are different from $R^T_{\rho/S}$. But, except for the negative $R^C_{\phi/S}$ in the deep transition zone, none of the harzburgite compositional velocity ratios are distinguishable from thermal values. Reducing the iron-content of pyrolite results in negative $R^C_{\rho/S}$ for the whole depth range 100–800 km. Only in the shallow lower-mantle where $R^C_{S/P}$ and $R^C_{\phi/S}$ are close to 1, are the velocity ratios due to a change in iron different from the thermal values. Hydrous pyrolite in the transition zone results in similar anomalies in all seismic parameters and compositional ratios close to 1, which distinguishes them, for all ratios, from the thermal values.

In summary, density/velocity ratios are the most indicative of compositional variations. Velocity/velocity ratios for the here investigated changes in composition only deviate from the thermal velocity ratio range for some compositions, and even then only in a limited depth range. Unfortunately, density estimates generally have larger uncertainties than seismic velocities.

A comparison with published seismic $R_{S/P}$, $R_{\phi/S}$, and $R_{\rho/S}$ (Forte and Mitrovica, 2001; Forte et al., 1993, 1994; Masters et al., 2000; Robertson and Woodhouse, 1996, 1997; Su and Dziewonski, 1997) shows that most of the values fall within the large range that may be expected due to temperature variations only. This makes it difficult to separate possible compositional effects from thermal effects. Only the low to negative values of $R_{\rho/S}$ found in the shallow upper-mantle are inconsistent with thermal structure, and may be the signature of Fe-depleted lithosphere, resulting in negative, composition dominated, density

variations and positive, temperature dominated, velocity variations (Forte et al., 1995). Low (0–0.2) $\partial \ln V_\phi / \partial \ln V_S$, found above 400 km depth (Masters et al., 2000; Su and Dziewonski, 1997), are only compatible with quite high temperatures and cannot be explained with any of the compositional models we tested. It is possible that the observed bulk-to-shear velocity ratios are influenced by the presence of fluids in the shallow mantle or by seismic anisotropy.

## 5. Conclusions

Using a compilation of published mineral physics data, we analyzed the uncertainties of forward calculated upper-mantle seismic velocities and density and their sensitivity to variations in temperature and composition. This analysis elucidates the potential and limitations of a thermal and/or compositional interpretation of upper-mantle seismic structure.

Temperature sensitivity of seismic velocity and density decreases with increasing depth. An additional decrease in sensitivity occurs in the wadsleyite stability field for velocity and in the ringwoodite stability field for density. Temperature derivatives for pyrolite and piclogite compositions are very similar. In the upper-mantle, anelasticity introduces strong temperature dependence in the temperature derivatives of $V_P$ and $V_S$. As a result, positive and negative velocity anomalies of the same amplitude relative to the same reference model, translate to different size thermal anomalies. Thus, it is necessary to know absolute seismic velocities for a thermal interpretation. In the lower-mantle, the importance of anelasticity reduces considerably, and interpreting velocity anomalies in terms of thermal anomalies becomes feasible. $V_\phi$ and density are a factor of 2 to 5 less sensitive to variations in temperature than $V_P$ and $V_S$, requiring a significantly better resolution of bulk sound or density than shear velocity if temperature is to be inferred.

Seismic velocities of pyrolite, piclogite and harzburgite differ by about 1%. Variations in iron content compatible with those found in common xenoliths and mantle peridotites, result in velocity anomalies in this same range. MORB and hydrated mantle compositions have larger, but most likely localized, effects. At depths less than about 400 km most compositional effects are small compared to the effect of a several 100° temperature change. At larger depths, the effect of composition becomes more important due to the lower sensitivity of seismic velocities to temperature. Taking into account compositional changes where expected may be useful in forward modelling tests, for example, in subduction zones and the overlying mantle wedge.

The uncertainties in elastic and anelastic parameters for mantle minerals introduce an uncertainty in temperatures inferred from seismic velocities of ±100 °C above 400 km and ±250 °C in the shallow lower-mantle. This assumes that seismic structure is well resolved, and composition known. Although uncertainties in anelasticity parameters are large, not taking anelastic effects into account introduces a larger error in upper-mantle temperature estimates. We find that, due to the limited sensitivity to composition, P- and S-wave velocities above the olivine–wadsleyite phase transition (around 400 km) can be inverted for thermal structure. The trade-off between phase transition depth and temperature and uncertainties in the phase diagrams and their dependence on composition make an inversion of the seismic velocity models in the transition zone unreliable at the moment. A use of the data for forward modeling and testing against seismic observations is however possible also at these depths.

Where anelasticity is important, the non-linear dependence of velocity on temperature makes absolute velocities required for an interpretation. Global one-dimensional seismic models form the basis for most seismic velocity models. To a first approximation these models agree with a pyrolitic mantle with temperatures following a 1300 °C adiabat. However, small differences (0.5–1%) between the mineralogical and seismic models map into large temperature differences (several 100 °C). It is not clear whether the seismic differences are resolved by the data, especially in the transition zone. A better understanding of the physical conditions that average seismic models is necessary for the interpretation of upper-mantle velocity models.

Under some conditions, the difference in sensitivity of bulk sound and density to thermal and compositional variations is different enough from the sensitivity of $V_P$ and $V_S$, that a separation of the two effects may be feasible when different data are combined. However, in many cases heterogeneity ratios due to

changes in composition fall within the wide range of values that are possible for reasonable temperature variations. Negative $\partial \ln V_S / \partial \ln V_P$ ratios are not expected for common upper-mantle compositions. Negative $\partial \ln \rho / \partial \ln V_S$ and $\partial \ln V_\phi / \partial \ln V_S$ may occur associated with subducted slabs. Of all ratios, $\partial \ln \rho / \partial \ln V_S$ show the least overlap for thermal and compositional structure. Except for shallow mantle density–velocity ratios, most of the reported upper-mantle heterogeneity ratios fall within the thermal range, although this does not rule out the presence of compositional variations.

## Acknowledgements

We thank Ian Jackson and Jeannot Trampert for their critical and thorough reviews, which stimulated significant improvements of the manuscript. This is ETH-Contribution No. 1301.

## Appendix A

The anharmonic velocities are calculated at given pressure and temperature ($P$, $T$) conditions by extrapolating density and the anharmonic moduli, first in temperature and then, along an adiabat, in pressure. Pressure is converted to depth using the pressure profile of the PREM model.

For each mineral, the adiabat that passes through the desired $P$, $T$ point is found. The adiabats are calculated using the following expression:

$$\left(\frac{\partial T}{\partial P}\right)_S = \left(\frac{\alpha T}{\rho C_P}\right)_{T,P_0} \left(\frac{\rho_0}{\rho}\right)^m$$

where the term $(\rho_0/\rho)^m$ represents a high pressure correction for $\alpha$ (Chopelas and Boehler, 1992). Above the Debye temperatures of minerals, $m = (\partial \ln \alpha / \partial \ln V)_T + 1$, where $(\partial \ln \alpha / \partial \ln V)_T$ (i.e. the Anderson–Grüneisen parameter) $\cong 5.5$ for most minerals in the mantle (Chopelas and Boehler, 1989). Assuming that the Anderson–Grüneisen parameter is constant is a reasonable approximation in the pressure range of the upper-mantle, even though a decrease proportional to compression $V/V_0$ is observed at increasing pressure (Chopelas and Boehler, 1992). Density and the elastic moduli are extrapolated to the potential temperature (surface temperature) $T_{pot}$ of this adiabat:

$$\rho(T_{pot}, P_0) = \rho(T_0, P_0) \exp\left[-\int_{T_0}^{T_{pot}} \alpha(T')\, dT'\right],$$

$$M(T_{pot}, P_0) = M(T_0, P_0) + \left(\frac{\partial M}{\partial T}\right)_P (T_{pot} - T_0)$$

where $M$ is an elastic modulus, i.e. $K_S$ or $G$. Pressure derivatives $M'$ are also extrapolated to high temperature following the procedure of Duffy and Anderson (1989):

$$M'(T) = M'(T_0) \exp\left[\int_{T_0}^{T} \alpha(T')\, dT'\right].$$

For the extrapolation in pressure a finite-strain formulation is adopted:

$$P = -(1-2\varepsilon)^{5/2}\left(C_1\varepsilon + \tfrac{1}{2}C_2\varepsilon^2 + \tfrac{1}{6}C_3\varepsilon^3 + \cdots\right)$$

The Eulerian strain,

$$\varepsilon = \frac{1}{2}\left[1 - \left(\frac{\rho(T,P)}{\rho(T_{pot},P_0)}\right)^{2/3}\right],$$

provides density at the chosen $P$ and $T$. The series is truncated to third-order, by setting $C_3 = 0$. The coefficients are: $C_1 = 3K_{S,0}$, and $C_2 = 9K_{S,0}(4 - K'_S)$, where $K_{S,0} = K_S(T_0, P_0)$, and $K'_S$ is the pressure derivative of $K_S$. $C_3 = 27K_{S,0}[K_{S,0}K''_S - K'_S(7 - K'_S) + 143/9] = 0$ constrains $K''_S$, the second pressure derivative of $K_S$.

The moduli at the selected $P$, $T$ conditions are determined from

$$K_S + \tfrac{4}{3}G = (1-2\varepsilon)^{5/2}(L_1 + L_2\varepsilon + \tfrac{1}{2}L_3\varepsilon^2),$$

and

$$G = (1-2\varepsilon)^{5/2}(M_1 + M_2\varepsilon + M_3\varepsilon^2).$$

The coefficients are

$$L_1 = K_{S,0} + \tfrac{4}{3}G_0,\ L_2 = 5L_1 - 3K_{S,0}(K'_S + \tfrac{4}{3}G')$$

and

$$L_3 = 9K_{S,0}^2(K''_S + \tfrac{4}{3}G'') - 3L_2\left(K'_S - 4\right) + 5L_1(3K'_S - 5)$$

Table A.1
Elasticity parameters of mantle minerals

| Mineral | $\rho$ (g/cm) | $K_S$ (GPa) | $G$ (GPa) | $K'_S$ | $G'$ | $\partial K_S/\partial T$ (GPa/K) | $\partial G/\partial T$ (GPa/K) |
|---|---|---|---|---|---|---|---|
| Olivine | $3.222 + 1.182X_{Fe}$ | 129 (±1%) | $81 - 31X_{Fe}$ (±1%) | 4.2 (±3%) | 1.4 (±7%) | −0.017 (±17%) | −0.014 (±17%) |
| Wadsleyite (β-phase) | $3.472 + 1.24X_{Fe}$ | 172 (±1%) | $112 - 40X_{Fe}$ (±1.5%) | 4.5 (±5%) | 1.5 (±10%) | −0.014 (±25%) | −0.014 (±25%) |
| Ringwoodite (γ-phase) | $3.548 + 1.30X_{Fe}$ | $185 + 35X_{Fe}$ (±1%) | $120.4 - 28X_{Fe}$ (±1.5%) | 4.1 (±10%) | 1.3 (±15%) | −0.024 (±20%) | −0.015 (±20%) |
| Clinopyroxenes Di–cEn–He | $3.277 + 0.38X_{Fe}$ | $105 + 12X_{Fe}$ (±1%) | $67 - 6X_{Fe}$ (±2%) | 6.2 $-1.9X_{Fe}$ (±10%) | 1.7 (±15%) | *−0.013 (±25%)* | *−0.010 (±25%)* |
| Jadeite | 3.32 | 126 (±1%) | 84 (±2%) | 5.0 (±10%) | *1.7 (±15%)* | −0.016 (±20%) | −0.013 (±25%) |
| Orthopyroxenes En–Fs | $3.215 + 0.799X_{Fe}$ | $109 + 20X_{Fe}$ (±2%) | $75 + 10X_{Fe}$ (±2%) | 7.0 (±20%) | 1.6 (±15%) | *−0.027 (±25%)* | *−0.012 (±25%)* |
| Garnet Py–Mj–Alm | $3.565 + 0.76X_{Alm} - 0.05X_{Mj}$ | $171 + 15X_{Alm} - 5X_{Mj}$ (±1%) | $92 + 7X_{Alm} - 5X_{Mj}$ (±2%) | $4.4 + 1.4X_{Mj}$ (±10%) | $1.4 + 0.3X_{Mj}$ (±15%) | −0.019 (±20%) | −0.010 (±25%) |
| Ca-Garnet (Grossular) | 3.597 | 168 (±1%) | 107 (±1%) | 5.2 (±10%) | 1.6 (±15%) | −0.016 (±20%) | −0.012 (±25%) |
| Na-majorite | 3.926 | 187 (±3%) | 115 (±3%) | 5.0 (±15%) | *1.6 (±15%)* | *−0.016 (±25%)* | *−0.015 (±25%)* |
| Mg-perovskite | $4.107 + 1.07X_{Fe}$ | 263 (±1%) | 175 (±2%) | 4.0 (±5%) | 1.8 (±15%) | −0.017 (±20%) | −0.029 (±20%) |
| Ca-perovskite | 4.210 | 236 (±2%) | 165 (±2%) | 4.4 (±10%) | 2.5 (±20%) | −0.022 (±25%) | −0.023 (±25%) |
| Mg-wustite | $3.584 + 2.28X_{Fe}$ | 162 (±1%) | $130 - 77X_{Fe}$ (±2%) | 4.0 (±10%) | 2.35 (±20%) | −0.021 (±20%) | −0.024 (±25%) |
| Ilmenite | $3.810 + 1.1X_{Fe}$ | 212 (±1%) | $132 - 41X_{Fe}$ (±2%) | 5.6 (±20%) | *1.7 (±15%)* | *−0.017 (±25%)* | *−0.017 (±25%)* |
| Coesite | 2.911 | 98 (±1%) | 61.7 (±1%) | 4.3 (±20%) | 1.5 (± 20%) | −0.015 (±30%) | −0.015 (±30%) |
| Stishovite | 4.289 | 294 (±1%) | 217 (±1%) | 5.3 (±15%) | 1.8 (±15%) | −0.034 (±20%) | −0.018 (±25%) |
| Corundum | 3.988 | 257 (±2%) | 162 (±2%) | 4.4 (±15%) | 1.8 (±15%) | −0.014 (±25%) | −0.019 (±25%) |
| Hydrous wadsleyite | $3.300 + 1.24X_{Fe}$ | 153 (±3%) | $105 - 40X_{Fe}$ (±4.5%) | 4.0 (±20%) | – | – | – |
| Hydrous ringwoodite | $3.470 + 1.30X_{Fe}$ | $155 + 35X_{Fe}$ (±3%) | $108.0 - 28X_{Fe}$ (±3%) | 5 (±20%) | – | – | – |

$\rho$: density; $K_S$: bulk modulus; $G$: shear modulus, $K'_S$ and $G'$: pressure derivatives of the moduli; $\partial K_S/\partial T$ and $\partial G/\partial T$: temperature derivatives of the moduli; $X_{Fe}$: mole fraction of iron; $X_{Alm}$, $X_{Mj}$: mole fractions of almandine and majorite in garnet solid solution. Di: diopside; cEn: clinoEnstatite; He: hedenbergite; En: enstatite; Fs: ferrosilite; Py: pyrope, Mj: majorite; Alm: almandine. Entries in italics are non-experimental values (elasticity systematics). Data are from the compilation by Vacher et al. (1998) as well as the following more recent references: for olivine (Zha et al., 1998); for wadsleyite (Katsura et al., 2001; Li and Liebermann, 2000; Li et al., 1998); for ringwoodite (Jackson et al., 2000; Sinogeikin et al., 1998a; Sinogeikin et al., 1998b); for orthopyroxene (Flesch et al., 1998); for garnets (Chen et al., 1999; Conrad et al., 1999; Gwanmesia et al., 2000; Morishima et al., 1999; Sinogeikin and Bass, 2000; Zhang et al., 1999); for perovskite (Karki and Stixrude, 1999; Saxena et al., 1999; Sinelnikov et al., 1998); for magnesiowüstite (Fei, 1999; Zha et al., 2000); for coesite (Angel et al., 2001b); for stishovite (Li et al., 1996; Liu et al., 1999); for corundum (Liebermann, 2000); for hydrous wadsleyite and hydrous ringwoodite (Inoue et al., 1998; Kudoh and Inoue, 1998; Yusa et al., 2000). Thermal expansions ($\alpha$) in terms of polynomials of temperature are from Saxena and Shen (1992).

and

$$M_1 = G_0,\ M_2 = 5M_1 - 3K_{S,0}G',$$

and

$$M_3 = 9K_{S,0}^2G'' - 3M_2(K_S' - 4) + 5M_1(3K_S' - 5)$$

It is assumed that $G'' = 0.631K''$. This equation is derived from Stacey's (1992) relation between bulk and shear modulus.

Hashin–Strikman averaging yields $\rho$, $K_S$ and $G$ at $P$, $T$ for a composite mineralogy. These parameters determine anharmonic $V_P$, $V_S$ and $V_\phi$. The effect of anelasticity is included as follows:

$$V(P, T, X, \omega) = V_{anh}(P, T, X)\left[1 - \frac{Q^{-1}(\omega, T)}{2\tan(\pi a/2)}\right],$$

where $V$ is $V_P$, $V_S$ or $V_\phi$, and $X$ stands for composition. The other parameters are anelasticity parameters, $Q$ is $Q_S$ for $V_S$, $QK$ for $V_\phi$ or $Q_P$ given by $Q_P^{-1} = (1 - \lambda)Q_K^{-1} + \lambda Q_\mu^{-1}$ with $\lambda = 4/3(V_S/V_P)^2$ for $V_P$. $\omega$ is frequency and $a$ the exponent describing the frequency dependence of attenuation.

## Appendix B

The mineral elasticity data set (Table A.1) is obtained starting from the compilation of Vacher et al. (1998) and updated with new high temperature–high pressure experiments that better constrain the elasticity of the mantle minerals. In particular, the employment of sophisticated in situ analysis techniques (such as X-ray diffraction with third generation of synchroton rings) has improved the quality of the data (Fiquet, 2001). At the same time, the progress of theoretical calculations (ab initio, first principle), which work well for the lower-mantle minerals (Karki et al., 2001; Oganov et al., 2001), expands our knowledge of mineral high pressure and high temperature behavior. For example, a good agreement between theoretical calculations and experimental data of the pressure derivatives $K_S'$ and $G'$ for Mg-perovskite has been found (Karki and Stixrude, 1999). Quite big uncertainties, however, remain in the thermal expansion coefficients and temperature derivatives of $K_S$ and $G$. An example is the case for $\partial K_S/\partial T$ of wadsleyite for which two recent experiments get quite different values (Katsura et al., 2001; Li et al., 1998). Katsura's experiment has been performed at ambient pressure and has smaller uncertainties than Li et al. (at 7 GPa and 873 K), but the cross effect of pressure on the temperature derivatives is not taken into account. In our compilation larger uncertainties have been assumed for data performed at high pressure, but ambient temperature or vice versa. For some minerals, experimental results for temperature derivatives are not available. In these cases, we still use the elasticity systematics of Duffy and Anderson (1989). In order to compare all the data available, experimental isothermal bulk moduli ($K_T$) have been converted in adiabatic ($K_S$) using their thermodynamic relation.

In Table A.1 the adopted elasticity values and the estimated uncertainties considering all quoted studies are reported. We compared results inferred from different techniques that usually have some discrepancies. For instance, for $K_S'$ of pyrope the Brillouin scattering technique gives lower values (3.22 in Conrad et al., 1999; 4.1 in Sinogeikin and Bass, 2000) than X-ray diffraction experiments (4.4 in Zhang et al., 1999) and ultrasonic techniques ($K_S' = 5.3$ in Chen et al., 1999). Therefore, global uncertainties given in Table A.1 are usually larger than the reported experimental uncertainties.

Further note, the strong non-linearity of the orthopyroxene bulk modulus with pressure, that requires a fourth-order finite-strain to fit the data (Flesch et al., 1998). In the lower-mantle, the magnesiowustite shear modulus also shows a non-linear behavior with pressure and a 4$E$ approximation fits the data better. However, to keep a uniform approach, we use the values fitted with a 3$E$ finite-strain equation, and increase the uncertainties.

## References

Angel, R.J., Frost, D.J., Ross, N.L., Hemley, R., 2001a. Stabilities and equations of state of dense hydrous magnesium silicates. Phys. Earth Planet. Int. 127, 181–196.

Angel, R.J., Mosenfelder, J.L., Shaw, C.S.J., 2001b. Anomalous compression and equation of state of coesite. Phys. Earth Planet. Int. 124, 71–79.

Bass, J.D., Anderson, D.L., 1984. Composition of the upper-mantle: geophysical test of two petrological models. Geophys. Res. Lett. 11, 237–240.

Béjina, F., Jaoul, O., Liebermann, R.C., 1999. Activation volume of Si diffusion in San Carlos olivine: implications for upper-mantle rheology. J. Geophys. Res. 104, 25529–25542.

Bina, C.R., Helffrich, G.R., 1994. Phase transition clapeyron slopes and transition zone seismic discontinuity topography. J. Geophys. Res. 1999, 15853–15860.

Birch, F., 1952. Elasticity and constitution of the Earth's interior. J. Geophys. Res. 57, 227–287.

Catti, M., 2001. High-pressure stability, structure and compressibility of Cmcm-$MgAl_2O_4$: an ab initio study. Phys. Chem. Miner. 28, 729–736.

Chen, G., Cooke, J.A., Gwanmesia, G.D., Liebermann, R.C., 1999. Elastic wave velocities of $Mg_3Al_2Si_3O_{12}$-pyrope garnet to 10 GPa. Am. Mineralogist 84, 384–388.

Chopelas, A., Boehler, R., 1989. Thermal expansion measurements at very high pressure, systematics, and a case for a chemically homogeneous mantle. Geophys. Res. Lett. 16, 1347–1350.

Chopelas, A., Boehler, R., 1992. Thermal expansivity in the lower-mantle. J. Geophys. Res. 19, 1983–1986.

Conrad, P.G., Zha, C.S., Mao, H., Hemley, R.J., 1999. The high-pressure single-crystal elasticity of pyrope, grissular and andradite. Am. Mineralogist 84, 374–383.

Davies, G.F., Dziewonski, A.M., 1975. Homogeneity and constitution of the Earth's lower-mantle and outer core. Phys. Earth Planet. Int. 10, 336–343.

Deal, M.M., Nolet, G., van der Hilst, R.D., 1999. Slab temperature and thickness from seismic tomography. Method and application to Tonga. J. Geophys. Res. 104, 28803–28812.

Deschamps, F., Snieder, R., Trampert, J., 2001. The relative density-to-shear velocity scaling in the uppermost mantle. Phys. Earth Planet. Int. 124, 193–211.

Deschamps, F., Trampert, J., Snieder, R., 2002. Anomalies of temperatures and iron in the uppermost mantle inferred from gravity data and tomographic models, Phys. Earth Planet. Int. 129, 245–264.

Drake, M.J., Righter, K., 2002. Determining the composition of the Earth. Nature 416, 39–44.

Duffy, T.S., Anderson, D.L., 1989. Seismic velocities in mantle minerals and the mineralogy of the upper-mantle. J. Geophys. Res. 94, 1895–1912.

Duffy, T.A., Zha, C.S., Downs, R.T., Mao, H.K., Hemley, R.J., 1995. Elasticity of forsterite to 16 GPa and the composition of the upper-mantle. Nature 378, 170–173.

Durek, J.J., Ekstrom, G., 1996. A radial model of anelasticity consistent with long-period surface-wave attenuation. Bull. Seismological Soc. Am. 86, 144–158.

Dziewonski, A.M., Anderson, D.L., 1981. Preliminary reference Earth model. Phys. Earth Planet. Int. 25, 297–356.

Dziewonski, A.M., Hales, A.L., Lapwood, E.R., 1975. Parametrically simple Earth models consistent with geophysical data. Phys. Earth Planet. Int. 10, 12–48.

Fei, Y., 1999. Effect of temperature and composition on the bulk modulus of (Mg, Fe)O. Am. Mineralogist 84, 272–276.

Fiquet, G., 2001. Mineral phases of the Earth's mantle. Z. Kristallogr. 216, 248–271.

Flesch, L.M., Li, B., Liebermann, R.C., 1998. Sound velocities of polycrystalline $MgSiO_3$-orthopyroxene to 10 GPa at room temperature. Am. Mineralogist 83, 444–450.

Forte, A.M., Mitrovica, J.X., 2001. Deep-mantle high viscosity flow and thermochemical structure inferred from seismic and geodynamic data. Nature 410, 1049–1056.

Forte, A.M., Perry, H.K.C., 2000. Geodynamic evidence for a chemically depleted continental tectosphere. Science 290, 1940–1944.

Forte, A.M., Peltier, W.R., Dziewonski, A.M., 1993. Dynamic surface-topography—a new interpretation based upon mantle flow models derived from seismic tomography. Geophys. Res. Lett. 20, 225–228.

Forte, A.M., Woodward, R.L., Dziewonski, A.M., 1994. Joint inversion of seismic and geodynamic data for models on three-dimensional mantle heterogeneity. J. Geophys. Res. 99, 21857–21887.

Forte, A.M., Dziewonski, A.M., O'Connell, R.J., 1995. Thermal and chemical heterogeneity in the mantle: a seismic and geodynamic study of continental roots. Phys. Earth Planet. Int. 92, 42–55.

Gaherty, J.B., Hager, B.H., 1994. Compositional versus thermal buoyancy and the evolution of subducted lithosphere. Geophys. Res. Lett. 21, 141–144.

Gaherty, J.B., Kato, M., Jordan, T.H., 1999a. Seismological structure of the upper-mantle: a regional comparison of seismic layering. Phys. Earth Planet. Int. 110, 21–41.

Gaherty, J.B., Wang, Y., Jordan, T.H., Weidner, D.J., 1999b. Testing plausible upper-mantle compositions using fine-scale models of the 410-km discontinuity. Geophys. Res. Lett. 26, 1641–1644.

Getting, I.C., Dutton, S.J., Burnley, P.C., Karato, S.I., Spetzler, H.A., 1997. Shear attenuation and dispersion in MgO. Phys. Earth Planet. Int. 99, 249–257.

Goes, S., Govers, R., Vacher, P., 2000. Shallow mantle temperatures under Europe from P and S wave tomography. J. Geophys. Res. 105, 11153–11169.

Goes, S., van der Lee, S., 2002. Thermal structure of the North American uppermost mantle inferred from seismic tomography, J. Geophys. Res. 107, 10.1029/2000JB000049.

Gudmundsson, O., Sambridge, M., 1998. A regionalized upper-mantle (RUM) seismic model. J. Geophys. Res. 103, 7121–7136.

Gwanmesia, G.D., et al., 2000. Elasticity of the pyrope ($Mg_3Al_2Si_3O_{12}$)–majorite ($MgSiO_3$) garnets solid solution. Phys. Chem. Miner. 27, 445–452.

Herzberg, C., Zhang, J., 1996. Melting experiments on anhydrous peridotite KLB-1: compositions of magmas in the upper-mantle and transition zone. J. Geophys. Res. 101, 8271–8295.

Herzberg, C., Ratteron, P., Zhang, J., 2000. New experimental observations on the anhydrous solidus for peridotite KLB-1. Geochem. Geophys. Geosyst. 1, paper no. 2000GC000089.

Hirose, K., Fei, Y., Ma, Y., Mao, H., 1999. The fate of the subducted basaltic crust in the Earth's lower-mantle. Nature 397, 53–56.

Hirschmann, M.M., 2000. Mantle solidus: experimental constraints and the effects of peridotite composition, Geochem. Geophys. Geosyst. 1, paper no. 2000GC000070.

Humphreys, E.D., Dueker, K.G., 1994. Physical state of the western US upper-mantle. J. Geophys. Res. 99, 9635–9650.

Inoue, T., Weidner, D.J., Northrup, P.A., Parise, J.B., 1998. Elastic properties of hydrous ringwoodite (γ-phase) in $Mg_2SiO_4$. Earth Planet. Sci. Lett. 160, 107–113.

Irifune, T., 1987. An experimental investigation of the pyroxene-garnet transformation in a pyrolite composition and its bearing on the constitution of the mantle. Phys. Earth Planet. Int. 45, 324–336.

Irifune, T., Ringwood, A.E., 1987a. Phase transformations in a harzburgite composition to 26 GPa: implications for dynamical behaviour of the subducting slab. Earth Planet. Sci. Lett. 86, 365–376.

Irifune, T., Ringwood, A.E., 1987b. Phase transformations in primitive MORB and pyrolite compositions to 25 GPa and some geophysical implications. High-Pressure Research in Mineral Physics (AGU), pp. 231–242.

Irifune, T., Ringwood, A.E., 1993. Phase-transformations in subducted oceanic-crust and buoyancy relationnships at depths of 600–800 km in the mantle. Earth Planet. Sci. Lett. 117, 101–110.

Ishii, M., Tromp, J., 1999. Normal-mode and free-air gravity constraints on lateral variations in velocity and density of Earth's mantle. Science 285, 1231–1236.

Ita, J., Stixrude, L., 1992. Petrology, elasticity and composition of the mantle transition zone. J. Geophys. Res. 97, 6849–6866.

Jackson, I., 1993. Dynamic compliance from torsional creep and forced oscillation tests: an experimental demonstration of linear viscoelasticity. Geophys. Res. Lett. 20, 2115–2118.

Jackson, I., 1998. Elasticity, composition and temperature of the Earth's lower-mantle; a reappraisal. Geophys. J. Int. 134, 291–311.

Jackson, I., 2000. Laboratory measurements of seismic waves dispersion and attenuation: recent progress. Earth's deep interior. Mineral Physics and Tomography from the Atomic to the Global Scale (AGU), pp. 265–289.

Jackson, I., Ridgen, S.M., 1998. Composition and temperature of the Earth's mantle: seismological models interpreted through experimental studies of Earth materials. In: Jackson, I. (Ed.), The Earth's Mantle: Composition, Structure and Evolution. Cambridge University Press, UK, pp. 405–460.

Jackson, I., Patterson, M.S., Fitz Gerald, J.D., 1992. Seismic wave dispersion and attenuation in Aheim dunite: an experimental study. Geophys. J. Int. 108, 517–534.

Jackson, J.M., Sinogeikin, S.V., Bass, J.D., 2000. Sound velocities and elastic properties of γ-$Mg_2SiO_4$ at 873 K by Brillouin spectroscopy. Am. Mineralogist 85, 296–303.

Jackson, I., Fitz Gerald, J.D., Faul, U.H., Tan, B.H., 2002. Grain-size-sensitive seismic wave attenuation in polycrystalline olivine. J. Geophys. Res. 107 (B12), 2360, doi:10.1029/2001JB-001225..

Jaques, A., Green, D., 1980. Anhydrous melting of peridotite at 0–15 Kb pressure and the genesis of tholeitic basalts. Contrib. Mineral. Petrol. 73, 287–310.

Jordan, T.H., 1988. Structure and formation of the continental tectosphere. J. Petrol., Special Lithosphere Issue, pp. 11–37.

Karato, S.I., 1993. Importance of anelasticity in the interpretation of seismic tomography. Geophys. Res. Lett. 20, 1623–1626.

Karato, S.I., 1997. On the separation of crustal component from subducted oceanic lithosphere near the 660 km discontinuity. Phys. Earth Planet. Int. 99, 103–111.

Karato, S., Jung, H., 1998. Water, partial melting and the origin of the seismic low velocity and high attenuation zone in the upper-mantle. Earth Planet. Sci. Lett. 157, 193–207.

Karato, S.I., Jung, H., 2003. Effects of pressure on high-temperature dislocation creep in olivine. Philosophical Magazine A, 83, 401–414.

Karato, S.I., Karki, B.B., 2001. Origin of lateral variation of seismic wave velocities and density in the deep mantle. J. Geophys. Res. 106, 21771–21783.

Karki, B.B., Stixrude, L., 1999. Seismic velocities of major silicates and oxide phases of the lower-mantle. J. Geophys. Res. 104, 13025–13033.

Karki, B.B., Stixrude, L., Wentzkovitch, R.M., 2001. High-pressure elastic properties of major materials of Earth's mantle from first principles. Rev. Geophys. 39, 507–534.

Kato, M., Nakanishi, I., 2000. Upper-mantle velocity structure in the western Pacific rim estimated from short-period recordings at Matsushiro seismic array system. Earth Planets Space 52, 459–466.

Katsura, T., et al., 2001. Temperature derivatives of elastic moduli of $(Mg_{0.91}Fe_{0.09})SiO_4$ modified spinel. Phys. Earth Planet. Int. 124, 163–166.

Kennett, B.L.N., Engdahl, E.R., Buland, R.P., 1995. Constraints on seismic velocities in the Earth from travel times. Geophys. J. Int. 122, 108–124.

Kennett, B.L.N., Widiyantoro, S., van der Hilst, R.D., 1998. Joint seismic tomography for bulk sound and shear wave speed in the Earth's mantle. J. Geophys. Res. 103 (12), 469–493.

Kudoh, Y., Inoue, T., 1998. Effect of pressure on the crystal structure of hydrous wadsleyite, $Mg_{1.75}SiH_{0.75}O_4$. High Pressure–Temperature Research: Properties of Earth and Planetary Materials (AGU), pp. 517–521.

Laske, G., Masters, G., 1998. Surface-wave polarization data and global anisotropic structure. Geophys. J. Int. 132, 508–520.

Laske, G., Masters, G., Dziewonski, A.M., 2001. New Measurements of Radial Mode Eigenfrequencies, S32B-0629 (AGU abstract).

Li, B., Liebermann, R.C., 2000. Sound velocities of wadsleyite β-$(Mg_{0.88}Fe_{0.12})_2SiO_4$ to 10 GPa. Am. Mineralogist 85, 292–295.

Li, B., Liebermann, R.C., Weidner, D.J., 1998. Elastic moduli of wadsleyite (β-$Mg_2SiO_4$) to 7 GPa and 873 K. Science 281, 675–677.

Li, B., Liebermann, R.C., Weidner, D.J., 2001. *P–V–VP–VS–T* measurements on wadsleyite to 7 GPa and 873 K: implications for the 410-km seismic discontinuity. J. Geophys. Res. 106, 30575–30591.

Li, B., Ridgen, S.M., Liebermann, R.C., 1996. Elasticity of stishovite at high pressure. Phys. Earth Planet. Int. 96, 113–127.

Liebermann, R.C., 2000. Elasticity of mantle minerals (experimental studies). Earth's deep interior. Mineral Physics and Tomography from the Atomic to the Global Scale (AGU), pp. 181–199.

Litasov, K., Ohtani, E., Taniguchi, H., 2001. Melting relations of hydrous pyrolite in CaO–MgO–$Al_2O_3$–$SiO_2$–$H_2O$ system in the transition zone. Geophys. Res. Lett. 28, 1303–1306.

Lithgow-Bertelloni, C., 2001. The origin of lateral heterogeneity in the Earth's mantle. In: Proceedings of the Eleventh Annual V.M. Goldschmidt Conference (Abstract).

Liu, J., et al., 1999. Thermal equation of state of stishovite. Phys. Earth Planet. Int. 112, 257–266.

Masters, G., Laske, G., Bolton, H., Dziewonski, A.M., 2000. The relative behavior of shear velocity, bulk sound speed, and compressional velocity in the mantle: implications for chemical and thermal structures. Earth's deep interior. Mineral Physics and Tomography from the Atomic To The Global Scale (AGU), pp. 63–87.

McDonough, W.F., Sun, S., 1995. The composition of the Earth. Chem. Geol. 120, 223–253.

Minster, J.B., 1980. Anelasticity and attenuation. Physics of the Earth's interior, Soc. Italiana di Fisica, Bologna, Italy.

Montagner, J.P., 1998. Where can seismic anisotropy be detected in the earth's mantle? In boundary layers. Pure Appl. Geophys. 151, 223–256.

Montagner, J.P., Kennett, B.L.N., 1996. How to reconcile body-wave and normal-mode reference earth models? Geophys. J. Int. 125, 229–248.

Montagner, J.P., Tanimoto, T., 1990. Global anisotropy in the upper-mantle inferred from the regionalization of phase velocities. J. Geophys. Res. 95, 4797–4819.

Morishima, H., et al., 1999. The high-pressure and temperature equation of state of a majorite solid solution in the system of $Mg_4Si_4O_{12}$–$Mg_3Al_2Si_3O_{12}$. Phys. Chem. Minerals 27, 3–10.

Murakami, T., Yoshioka, S., 2001. The relation between the physical properties of the assumed pyrolite composition and depth distributions of seismic velocities in the upper-mantle. Phys. Earth Planet. Int. 125, 1–17.

Nolet, G., Zielhuis, A., 1994. Low S-velocities under the Tornquist–Teisseyre zone—evidence for water injection into the transition zone by subduction. J. Geophys. Res. 99, 15813–15820.

Nolet, G., Grand, S.P., Kennett, B.L.N., 1994. Seismic heterogeneity in the upper-mantle. J. Geophys. Res. 99, 23753–23766.

Oganov, A.R., Brodholt, J.P., 2000. High-pressure phases in the $Al_2SiO_5$ system and the problem of aluminous phase in the Earth's lower-mantle: ab initio calculations. Phys. Chem. Miner., 27.

Oganov, A.R., Brodholt, J.P., Price, G.D., 2001. The elastic constants of $MgSiO_3$ perovskite at pressures and temperatures of the earth's mantle. Nature 411, 934–937.

Paulssen, H., 1988. Evidence for small scale structure of the upper-mantle. Ph.D. thesis. Geologica Ultraiectina, Utrecth, pp. 1–109.

Poirier, J.P., Tarantola, A., 1998. A logarithm equation of state. Phys. Earth Planet. Int. 109, 1–8.

Revenaugh, J., Jordan, T.H., 1991. Mantle layering from ScS reverberations. Part 1. Waveform inversion of zeroth-order reverberations. J. Geophys. Res. 96, 19749–19762.

Ritsema, J., van Heijst, H.J., 2001. Automatic Measurements of Surface Wave Phase Velocities and Body-Wave Travel Times: New Data for New Seismic Reference Earth Models. S21B-03 (AGU Abstract).

Robertson, G.S., Woodhouse, J., 1996. Ratio of relative S to P velocity heterogeneity in the lower-mantle. J. Geophys. Res. 101, 20041–20052.

Robertson, G.S., Woodhouse, J., 1997. Comparison of P and S station corrections and their relationship to upper-mantle structure. J. Geophys. Res. 102, 27355–27366.

Romanowicz, B., Durek, J.J., 2000. Seismological constraints on attenuation in the Earth: a review. Earth's deep interior. Mineral Physics and Tomography from the Atomic to the Global Scale (AGU), pp. 161–179.

Saltzer, R.L., van der Hilst, R.D., Karason, H., 2001. Comparing P and S wave heterogeneity in the mantle. Geophys. Res. Lett. 28, 1335–1338.

Saxena, S.K., Dubrovinski, L.S., Tutti, F., Le Bihan, T., 1999. Equation of state of $MgSiO_3$ with the perovskite structure based on experimental measurement. Am. Miner. 84, 226–232.

Saxena, S.K., Shen, G., 1992. Assessed data on heat capacity, thermal expansion and compressibility for some oxides and silicates. J. Geophys. Res. 97, 19813–19825.

Shearer, P.M., 2000. Upper-mantle seismic discontinuities. Earth's deep interior. Mineral Physics and Tomography from the Atomic to the Global Scale (AGU), pp. 115–131.

Shearer, P.M., Flanagan, M.P., 1999. Seismic velocity and density jumps across the 410- and 660-kilometer discontinuities. Science 285, 1545–1548.

Shim, S.H., Duffy, T.D., Shen, G., 2000. The stability and *P–V–T* equation of state of $CaSiO_3$ perovskite in the Earth's lower-mantle. J. Geophys. Res. 105, 25955–25968.

Sinelnikov, Y.D., Chen, G., Neuville, D.R., Vaughan, M.T., Liebermann, R.C., 1998. Ultrasonic shear wave velocities of $MgSiO_3$ perovskite at 8 GPa and 800 K and lower-mantle composition. Science 281, 677–679.

Sinogeikin, S.V., Bass, J.D., 2000. Single-crystal elasticity of pyrope and MgO to 20 GPa by Brillouin spectroscopy in the diamond cell. Phys. Earth Planet. Int. 120, 43–62.

Sinogeikin, S.V., Bass, J.D., Katsura, T., 1998a. Elasticity of $(Mg, Fe)_2SiO_4$ spinel to transition zone pressures. EOS, Transactions Am. Geophys. Union 79, F861.

Sinogeikin, S.V., Katsura, T., Bass, J.D., 1998b. Sound velocities and elastic properties of Fe-bearing wadsleyite and ringwoodite. J. Geophys. Res. 103, 20819–20825.

Sobolev, S.V., et al., 1997. Upper-mantle temperatures and lithosphere-asthenosphere system beneath the French Massif Central constrained by seismic, gravity, petrological and thermal observations. Tectonophysics 275, 143–164.

Sobolev, S.V., et al., 1996. Upper-mantle temperatures from teleseismic tomography of French massif central including effects of composition, mineral reactions, anharmonicity, anelasticity and partial melt. Earth Planet. Sci. Lett. 139, 147–163.

Stacey, F.D., 1992. Physics of the Earth. 3rd ed. Brookfield Press, Brisbane.

Stacey, F.D., Isaak, D.G., 2001. Compositional constraints on the equation of state and thermal properties of the lower-mantle. Geophys. J. Int. 146, 143–154.

Stalder, R., Ulmer, P., 2001. Phase relations of a serpentine composition between 5 and 14 GPa: significance of clinohumite and phase E as water carriers into the transition zone. Contrib. Mineral. Petrol. 140, 670–679.

Stixrude, L., 1997. Structure and sharpness of phase-transitions and mantle discontinuities. J. Geophys. Res. 102, 14835–14852.

Su, W.J., Dziewonski, A.M., 1997. Simultaneous inversion for 3D variations in shear and bulk velocity in the mantle. Phys. Earth Planet. Int. 100, 135–156.

Tan, B.H., Jackson, I., Fitz Gerald, J.D., 2001. High-temperature viscoelasticity of fine-grained polycrystalline olivine. Phys. Chem. Minerals 28, 641–664.

Tralli, D.M., Ita, J., 1995. Regionalized temperature variations in the upper 400 km of the Earth's mantle. Phys. Earth Planet. Int. 91, 177–186.

Trampert, J., Vacher, P., Vlaar, N., 2001. Sensitivities of seismic velocities to temperature, pressure and composition in the lower-mantle. Phys. Earth Planet. Int. 124, 255–267.

Ulmer, P., 2001. Partial melting in the mantle wedge—the role of $H_2O$ in the genesis of mantle-derived 'arc-related' magmas. Phys. Earth Planet. Int. 127, 215–232.

Vacher, P., Mocquet, A., Sotin, C., 1996. Comparison between tomographic structures and models of convection in the upper-mantle. Geophys. J. Int. 124, 45–56.

Vacher, P., Mocquet, A., Sotin, C., 1998. Computation of seismic profiles from mineral physics: the importance of non-olivine components for explaining the 660 km depth discontinuity. Phys. Earth Planet. Int. 106, 275–298.

Vasco, D.W., Johnson, L.R., 1998. Whole earth structure estimated from seismic arrival times. J. Geophys. Res. 103, 2633–2671.

Wang, Y., Weidner, D.J., Guyot, F., 1996. Thermal equation of state of $CaSiO_3$ perovskite. J. Geophys. Res. 101, 661–672.

Webb, S.L., Jackson, I., Fitz Gerald, J.D., 1999. Viscoelasticity of the titanat perovskites $CaTiO_3$ and $SrTiO_3$ at high temperature. Phys. Earth Planet. Int. 115, 259–291.

Weidner, D.J., 1985. A mineral physics test of a pyrolite mantle. Geophys. Res. Lett. 12, 417–420.

Weidner, D.J., Wang, Y., 1998. Chemical- and Clapeyron-induced buoyancy at the 660 km discontinuity. J. Geophys. Res. 103, 7431–7441.

Yamazaki, D., Karato, S., 2001. Some mineral physics constraints on the rheology and geothermal structure of Earth's lower-mantle. Am. Mineralogist 86, 385–391.

Yamazaki, D., Kato, M., Yurimoto, H., Ohtani, E., Toriumi, M., 2000. Silicon self-diffusion in $MgSiO_3$ perovskite at 25 GPa. Phys. Earth Planet. Int. 119, 299–309.

Yasuda, A., Fujii, T., Kurita, K., 1994. Melting phase relations of an anhydrous mid-ocean ridge basalt from 3 to 20 GPa: implications for the behavior of subducted oceanic crust in the mantle. J. Geophys. Res. 99, 9401–9414.

Yusa, H., Inoue, T., Ohishi, Y., 2000. Isothermal compressibility of hydrous ringwoodite and its relation to the mantle discontinuities. Geophys. Res. Lett. 27, 413–416.

Zerr, A., Diegeler, A., Boehler, R., 1998. Solidus of the Earth's deep mantle. Science 281, 243–246.

Zha, C., Duffy, T.D., Downs, R.T., Mao, H., Hemley, R.J., 1998. Brillouin scattering and X-ray diffraction of San Carlos olivine: direct pressure determination to 32 GPa. Earth Planet. Sci. Lett. 159, 25–33.

Zha, C.S., Mao, H., Hemley, R.J., 2000. Elasticity of MgO and a primary pressure scale to 55 GPa. PNAS 97, 13494–13499.

Zhang, L., Ahsbahs, H., Kutoglu, A., Geiger, C.A., 1999. Single-crystal hydrostatic compression of synthetic pyrope, almandine, spessartine, grossular and andradite garnets at high pressures. Phys. Chem. Minerals 27, 52–58.